Application of a synthesis of PHREEQC and PoreFlow: Investigating the onset and development of wormholing during CO_2 sequestration in limestone

Naod Negash
Student No.: 3915263
45 ECTS

Primary Supervisor: Dr. Amir Raoof
Secondary Supervisor: Prof. Dr. Ruud Schotting

MSc Thesis
Earth Surface Water
Utrecht University

Abstract

In order to curb the effects of climate change as a result of greenhouse gas emissions, the IPCC has emphasized the role carbon-dioxide capture and storage (CCS) will need to have in the coming decades. Of the potential CCS sites are former oil fields and deep-sea reservoirs, some of which have high carbonate content. When CO_2 is dissolved in water it forms an acidic solution which will react with resident carbonate minerals (e.g. limestone), resulting in a change of the pore-structure of and upscaled pore-scale properties such as permeability. To that end, pore-network models coupled with reaction modules provide a useful tool to investigate the reactive transport of such systems. In this research a novel approach to model reactive transport using a pore-network model, PoreFlow (Raoof et al., 2013), and geochemical model, PHREEQC (Appelo and Parkhurst, 2013), is proposed and investigated in the context of CO_2 sequestration in limestone. The approach entails projecting a 3D pore-network to a 1D domain and coupling the two domains such that resulting changes in the 3D pore-network would be analogous to doing reactive transport directly on the network. The goal of this new approach is to greatly reduce computational costs, yet still retain physical relevance. To test the model validity, an attempt to realize the *wormholing* phenomenon is made, and related concepts such as optimum conditions for well-stimulation and Damköhler number are investigated. Both strengths and shortcomings are discussed, as well as possibilities and suggestions for further research to develop the model even more.

Contents

1 Introduction

Anthropogenic induced climate change is perhaps one of the most pressing issues we are faced with today. The influence of humans on the climate system is becoming increasingly clear and impactful, with the effects of climate change noticeable across the globe (IPCC AR5 Synthesis Report, 2014). Many of the observed changes in the Earth's climate since the 1950s have been described as unprecedented over the last centuries and even millennia. One of the main mitigation pathways highlighted in the IPCC AR5 Synthesis Report (2014) is the widespread deployment of carbon-dioxide capture and storage (CCS, i.e. CO_2-sequestration). The storage of CO_2 is not a new concept, an example being Sleipner gas field in the North Sea which has been storing CO_2 in the subsurface since 1996 and by 2008 has stored more than 10 Mt of CO_2 (Akervoll et al., 2009). However, despite its attractiveness as a solution to the high atmospheric CO_2 concentrations there are still some uncertainties in undertaking CCS due to the reactive nature of dissolved CO_2, including the promise of fail-safe retention (Mehmani et al., 2012; Boot-Handford et al., 2014; Ott and Oedai, 2015; Gao et al., 2017; Selvadurai et al., 2017). Due to the inherent complexity of the coupled processes associated with sequestering CO_2 (Akono et al., 2019), particularly in porous media with high carbonate content, in addition to relatively high costs associated with lab experiments (Raoof et al., 2013), there exists a great need for models that can predictively capture and quantitatively analyse the pore-scale processes (Gao et al., 2017; Smith et al., 2017).

One phenomenon of particular interest is the emergence of highly conductive channelized pores as a result of dissolution of the porous medium (e.g. carbonates), otherwise known as 'wormholing'. These unstable dissolution structures greatly increase pore conductivity, effectively increasing the local permeability and therefore possibly compromise the trapping capability of overlying caprock or may facilitate faster migration of the CO_2 plume when supercritical CO_2 is injected (Nogues et al., 2013). Research on wormhole formation has been studied relatively extensively in the past, usually with focus on well-stimulation and enhanced oil recovery (EOR) (e.g. Hoefner and Fogler, 1988; Daccord et al., 1993; Fredd and Fogler, 1998a; Golfier et al., 2001; Golfier et al., 2002; Cohen et al., 2008; Ott and Oedai., 2015). While quantitative modelling of the phenomenon has proven to be difficult (e.g. Fredd and Fogler, 1998a; Selvadurai et al., 2017; Gray et al., 2018), there is a generally good qualitative understanding of the different processes involved in wormhole formation. When injecting an acid into a porous substrate, there exists an interplay between the transport phenomena and the kinetics of reactions. This coupling of processes gives rise to a complex system from which various dissolution patterns (Fig. 1) have been observed in both experiments and numerical simulations (Fredd and Fogler, 1998a; Golfier et al., 2001). The dissolution patterns are dependent on both the characteristic times of reaction and advection/diffusion, and are classified into five categories: face dissolution, conical wormhole, dominant wormhole, ramified wormhole, and uniform dissolution. On the one hand face-dissolution occurs when the characteristic time of reaction is smaller than the time of advection/diffusion, and as such virtually all the acid is consumed when it enters the porous medium. This results in a dissolution pattern in which the face of the porous medium is dissolved, relative to the direction of flow, with the dissolution front progressing forward as the carbonate is dissolved. On the other hand, uniform dissolution occurs when the characteristic time of transport is much smaller than that of reaction, resulting in homogeneous dissolution. Wormholing occurs when there is a particular balance between the two characteristic times such that initial preferential flow paths are developed further but that less conductive pores don't receive as much acid. This has led to the concept of optimum flow rate for any given system (Wang et al., 1993; Mostofizadeh and Economides, 1994; Fredd and Fogler, 1998a; Cohen et al., 2008) with the objective of well-stimulation. This concept of optimum flow rate will be a key aspect in this research and will be elucidated in later sections.

It is clear that pore-scale models capable of modelling reactive transport are of vital importance to gain insights to pore-scale processes. Reactive transport in porous media is characterized by coupled physical and chemical processes: fluid transport brings acid to a reaction site, surface reactions cause dissolution of the medium, this in turn changes the transport properties, and the cycle continues. This in combination with both heterogeneity of the pore space and in mineral distribution makes modelling of such systems difficult. As a result, pore-scale reactive transport modelling can be quite computationally expensive (Xiong et al., 2016; Maheshwari et al., 2013; Smith et al., 2017) even for pore-network models. This limits the extent of the modelled domain, which has been shown to be an

important factor in modelling wormhole formation (Cohen et al., 2008). To that end creative new modelling techniques could be employed to reduce computational costs yet still be able to at least qualitatively, and perhaps also quantitatively, describe the pore-scale processes at an even larger scale than is currently done.

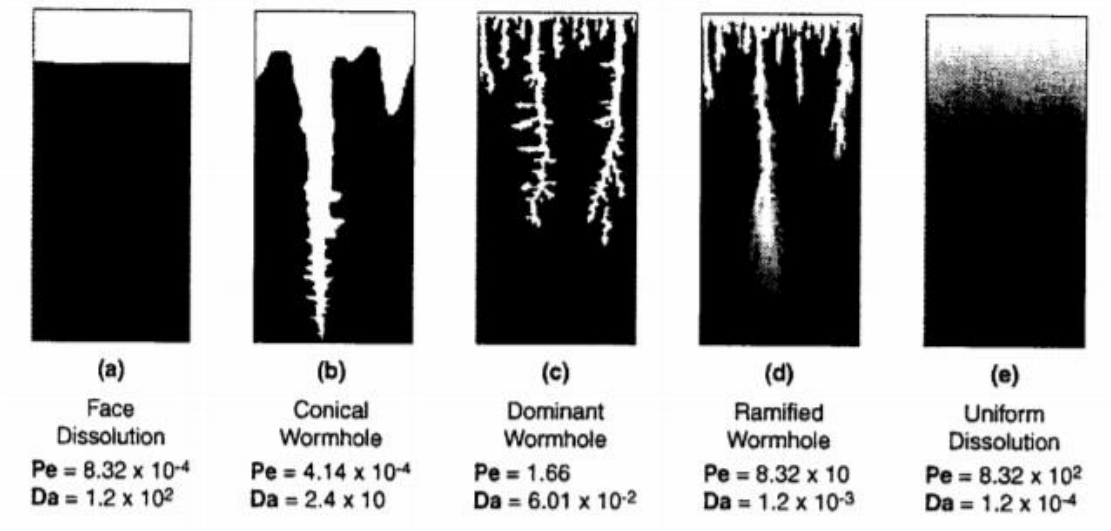

Figure 1 *The different types of dissolution patterns observed at different injections rates, and therefore also Damköhler number. For slower flow face dissolution takes place, and as flow rate increases wormholes begin to form. The ideal dissolution regime with respect to well stimulation is the dominant wormhole as it requires the least amount of acid to achieve a given permeability. Image from Golfier et al., 2001.*

1.1 Objectives

This leads to the objectives of this research. The primary goal of the research is to develop a coupled model capable of simulating single-phase reactive transport using a complex pore-network model (CPNM), PoreFlow (Raoof et al., 2013), and a (geo)chemical model, PHREEQC Version 3 (Parkhurst and Appelo, 2013). However, the approach is unique in that generally pore-network models used in reactive-transport calculate the reactions per individual pore body/throat. In our case the model effectively calculates 1D reactive transport of solutes through PHREEQC and transmits data on how much calcite is dissolved per 1D cell to PoreFlow. PoreFlow then uses the information to update the pore-network and transmits reactive-surface area data back to PHREEQC, an approach similar to that of Ameri et al. (2017). The coupling of the two models will be explained in greater detail in later sections, but basically this method would greatly reduce computational costs. The second objective is to test the capabilities of the model in capturing the wormholing phenomenon in a CO_2-water-calcite system at reservoir conditions. The investigation into wormholing will additionally be done by assessing the effect of temperature and mass transport limitations through various simulation conditions.

2 Background Information

In this section relevant background information is given regarding functions of the pore-network model used, PoreFlow, and the chemical model, PHREEQC. In addition, a brief review is given on reaction kinetics and mass transport limitation thereof, and the concept of optimal conditions for wormhole formation.

2.1 PoreFlow: A Complex Pore-Network Model

When modelling fluid or reactive transport at the pore scale, there are generally two approaches taken: direct modelling and pore-network modelling (Blunt et al., 2013). The former is done by discretizing the pore-space in a Cartesian grid, based on a 3D image of a sample, and running fluid-dynamical equations directly on that grid (e.g. Kang et al., 2006; Bijeljic et al., 2013; Gray et al., 2018). The key aspect of this approach is that it accurately represents the physical geometry of the pore space, limited only by the imaging technique, but therefore also has high computational costs associated with it (Blunt et al., 2013). Pore network models on the other hand idealize the pore space extracted from the scanned image into a network of pore bodies, represented as spheres, connected by pore throats, usually represented as cylinders. While compromising on accurate physical representation of a sample, it does have the benefit of being less computationally demanding yet retaining predictive capabilities.

In this section a brief overview of the pore-network model used in this research, PoreFlow (Raoof et al., 2013), is given. PoreFlow is a complex pore-network model capable of pore-network generation, modelling variably saturated flow, multi-component reactive and adsorptive transport, and more. One distinguishing feature of PoreFlow is that it can allow pores to have coordination numbers of up to 26, allowing for more realistic representation of natural porous media (Jivkov et al., 2013). Figure 2 illustrates how a given pore body can be connected to neighbouring pores. While this does better represent actual porous media than previous pore-network models in that it allows pores to have a coordination number greater than 6, it also gives rise to intersecting pore-throats which is physically unrealistic (Xiong et al., 2016). Nevertheless, it has shown to be able to accurately model the breakthrough curve of a tracer injection (Raoof et al., 2013) indicating that transport is well represented.

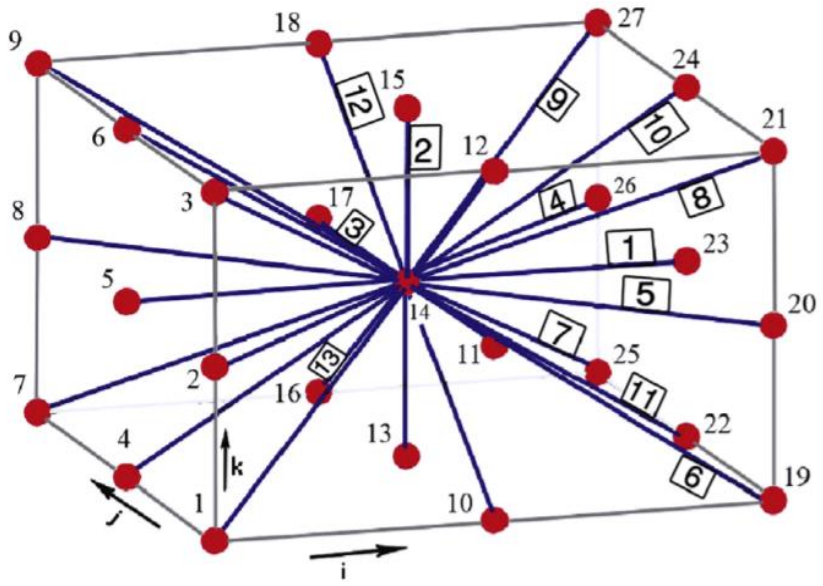

Figure 2 *A schematic representation of a small network consisting of three nodes (i.e. pore bodies) in each direction. The network shows all the possible connections a pore body can have, here for pore body 14, giving it a coordination number of 26. The numbers inside the squares denote the possible throat directions while the plain numbers denote pore bodies. Image from Raoof and Hassanizadeh, 2009.*

Flow in the network is simulated by means of a pressure gradient across the network. Flow within any given throat (Fig. 3) is described by the Hagen-Poiseuille equation (Eq. 1):

$$q_{ij} = g_{ij}(p_j - p_i) \quad (1)$$

where q_{ij} and g_{ij} are the discharge [$L^3\ T^{-1}$] and conductance [$L^4\ T\ M^{-1}$] of throat *ij*, respectively, and p_i and p_j are the fluid pressures [$M\ L^{-1}\ T^{-2}$] in pore bodies *i* and *j*, respectively. The assumption with using equation 1 is that flow is laminar, which is generally the case for flow in porous media. The conductance of a given throat is given by:

$$g_{ij} = \frac{\pi R_{ij}^4}{8\mu l_{ij}} \quad (2)$$

where R is the radius of throat *ij* [L], μ is the dynamic viscosity of the fluid [$M\ L^{-1}T^{-1}$], and l is the length of throat *ij* [L]. For steady-state incompressible flow, the sum of discharges of all pore throat connected to a given pore body must be zero to maintain continuity:

$$\sum_{j=1}^{z_i} q_{ij} = 0; \quad j = 1, 2, \ldots z_i \quad (3)$$

where z_i is the coordination number of pore body *i*.

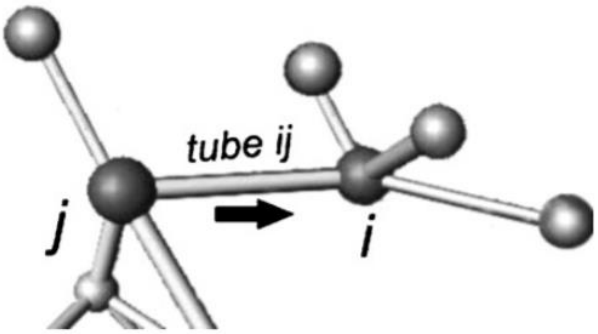

Figure 3 *Representation of connected pore bodies and associated subscripts. The arrow denotes the direction of the flow. Image from Raoof et al., 2012.*

Given that the total discharge through the network can easily be determined, the permeability can also be calculated using Darcy's law at any given time:

$$k = \frac{\mu Q_t}{A\Delta P/L} \quad (4)$$

where k is the intrinsic permeability [L^2], Q_t is the total discharge through the network [$L^3\ T^{-1}$], A is the cross-sectional area [L^2], L is the length of the network [L], and ΔP is the pressure gradient [$M\ L^{-1}\ T^{-2}$]. Since transport and reaction will be handled in PHREEQC, the transport and geochemical components of PoreFlow will not be discussed here.

As for network generation, PoreFlow uses a random elimination procedure to eliminate pore bodies and throats: initially the network contains all possible bodies and throats (Raoof and Hassanizadeh, 2009). This is done by assigning a set of 13 threshold numbers to every pore body for each direction axis, which are all between 0 and 1. Then a random number between 0 and 1 is generated for every throat and compared with the threshold number: if it is greater than the threshold number then the throat is 'closed', and if it is less then it is 'open'. They have also found there exists a critical threshold number below which not enough pores are connected and thus the conductivity is 0, which is 0.08. The

network generation procedure has proven to be quite good at reproducing representative networks. They generated a network with the same coordination number distribution (through optimization) as a representative network of a Fontainebleau sandstone sample reported in Al-Kharusi and Blunt (2006) and found good agreement with other network characteristics such as number of pore bodies and throats, mean coordination number, and number of inlet and outlet throats. With respect to throat radius calculation, the radius of a given throat is dependent on the two bodies it connects based on the scheme used in Acharya et al. (2004). For more detailed information of the pore-network generation and model description the reader is referred to Raoof and Hassanizadeh (2009) and Raoof et al. (2013).

2.2 PHREEQC

PHREEQC is a program designed to simulate chemical reactions in a variety of fields and environments, including geochemical applications (e.g. natural waters), laboratory experiments, and industrial processes (Parkhurst and Appelo, 2013). What makes PHREEQC appealing is that it contains a vast database of chemical equilibrium and several kinetic reactions, with the added benefit of easily appending or modifying reactions if necessary. Furthermore, its modular design facilitates synthesis with other transport models (Charlton and Parkhurst, 2011; Parkhurst and Wissmeier, 2015), and has therefore been incorporated in numerous models as a geochemical module such as PHAST and PHT3D. In addition to being a powerful chemical modelling tool, it can also simulate 1D transport in porous medial, making it ideal for the purpose of this research.

The types and sequence of calculations as stated in the PHREEQC Version 3 manual (Parkhurst and Appelo, 2013) are as follows: (1) initial solution/speciation calculations, (2) initial ion exchange calculations, (3) initial surface complexation calculations, (4) initial gas-phase calculations, (5) batch-reaction calculations (e.g. mixing, irreversible reactions, mineral equilibration) , (6) inverse-modelling calculations, (7) advective-transport calculations, (8) advective-dispersive-transport calculations, (9) cell batch-reaction calculations, (10) copy operations, (11) dump operations, and (12) delete operations. The calculations of interest to this research are 1, 5, 8, and 9.

PHREEQC calculates the speciation of a given solution composition by first assuming the system being in equilibrium, allowing for the system to be described by a set of non-linear equations based on variables called master unknowns. Subsequently, equilibrium is determined by means of a modified Newton-Raphson method used to solve the set of nonlinear equations (Parkhurst and Appelo, 1999). These equations are generally mole- and mass-balance laws, but also include functions for ionic strength and charge balances (and others), which generally contain mass-action laws defined in the database. Solving these equations (i.e. the functions reduce to zero) gives the equilibrium condition of the system. Furthermore, PHREEQC solves the set of equations by rewriting all aqueous species in terms of master species (and other master unknowns) using mass-action expressions (i.e. equilibrium expressions), reducing the number of unknowns that need to be determined. Master species include individual (aqueous) elements or element valence states, activity of the hydrogen ion, activity of (aqueous) electrons, and activity of water. For a more detailed review of calculations and precise description of the equations (without derivation) the reader is referred to the PHREEQC Version 2 manual (Parkhurst and Appelo, 1999).

Reactive transport in PHREEQC is done using the 1D advection-dispersion-reaction (ADR) equation (Eq. 5), which describes fluid flow through porous medium at the continuum scale (i.e. pore-scale phenomena are averaged and lumped together in constitutive macroscopic parameters such as dispersivity). The ARD equation has the form:

$$\frac{dC}{dt} = -v\frac{dC}{dx} + D_L\frac{d^2C}{dx^2} - \frac{dq}{dt} \qquad (5)$$

where C is molal concentration of a given solute [mol M^{-1}], t is time [T], v is the pore water velocity [L T^{-1}], x is distance [L], D_L the longitudinal dispersion coefficient [L^2 T^{-1}], and q is the concentration in the solid phase (number of moles per mass of pore water) [mol M^{-1}] . The first term on the right-hand side represents the convective transport of the solute, the second represents dispersive transport (due to the tortuous nature of porous media), and the third represents the effect of reaction(s). The dispersion coefficient is defined by:

$$D_L = D_e + \alpha_L \times v \quad (6)$$

where D_e is the effective diffusion coefficient [$L^2\ T^{-1}$], and α_L is the longitudinal dispersivity [L]. Equation 5 is solved using the split-operator method, with transport and reactions being calculated separately. For a given time-step the order of calculations is: (1) advection, (2) kinetic and equilibrium reactions, (3) dispersion, and (4) again kinetic and equilibrium reactions. In a split-operator scheme numerical stability and accuracy can be optimized by adjusting the time-step to the grid-size such that velocity is always equal to grid-size (Δx) divided by the time-step (Δt). As such the velocity per cell cannot be explicitly defined but is implicit in the definition of the time-step and cell-length. Furthermore, to avoid violation of the Courant condition and Von Neumann criterion several dispersions time-steps (and thus also reaction calculations) are calculated within a single advective timestep, such that $\sum \Delta t_D = t_A$, where Δt_D and Δt_A are the time-steps for dispersion and advection, respectively. Dispersion in PHREEQC is solved using an explicit finite difference scheme that is forward in time and central in space, and is therefore basically a mixing of adjacent cells (Parkhurst and Appelo, 1999) given by:

$$mixf = \frac{D_L \Delta t_A}{n(\Delta x)^2} \quad (7)$$

with n being the number of mixes performed within one advective time-step. This effectively leads to transport in PHREEQC being simulated as simply moving contents of one cell to the next for advection, and mixing with the neighbouring cells for dispersion, with dispersion and reaction calculations happening several times within one advective time-step. Possible limitations with using the transport capabilities of PHEEQC in investigating wormhole formation is that wormholes may give rise to non-Fickian transport (Ameri et al., 2017), and as such the validity of equation 5 is questionable. Again, for a more detailed description of transport in PREEQC the reader is referred to the PHREEQC Version 2 manual.

With respect to kinetic reactions, specifically defined kinetic rates are easily incorporated in PHREEQC through a built-in BASIC interpreter. The BASIC interpreter contains the rate expression, and a Runge-Kutta scheme (up to 5th order) solves the differential equation(s) over a time interval. The feedback of changing solution speciation on the rates is considered within an integration time interval. It uses the lower order schemes to determine an error-estimate based on user-defined error tolerance and reduces the time interval over which the integration is done if the tolerance is not met. This scheme is quite useful to achieve a solution when multiple reaction rates are defined with large discrepancies in change of rates as the reactions progress. The specifics of the reaction kinetics of calcite dissolution will be discussed in the following sub-section, and the rate expressions employed will be described in the Methods.

Also important to note is the solubility of gasses and solids at high pressures, such as in reservoirs for CO_2 sequestration. To simulate such conditions PHREEQC uses a modified Redlich-Rosenfield equation to determine the molar volumes of aqueous species and the Van der Waals equation to determine the fugacity coefficients of gasses (Appelo et al., 2014).

2.3 Chemical System and Reaction Kinetics

The kinetics of calcite dissolution have been studied quite extensively (e.g. Sjoberg, 1975; Plummer et al., 1978; Chou et al., 1989; Alkattan et al., 1998; Fredd and Fogler, 1998b; Pokrovsky et al., 2009; Peng et al., 2015). Chou et al. (1989) and Plummer et al. (1978) have determined three parallel pathways in which calcite dissolves, albeit with slight difference regarding the last pathway:

$$CaCO_3(s) + H^+ \leftrightarrow Ca^{2+} + HCO_3^- \quad (R1)$$

$$CaCO_3(s) + H_2CO_3^* \leftrightarrow Ca^{2+} + 2HCO_3^- \quad (R2)$$

$$CaCO_3(s) \leftrightarrow Ca^{2+} + CO_3^{2-} \quad (R3)$$

with the rate constants and activation energies given in table 1. Plummer et al. (1978) observed that backward reaction was only dependent on R3, yet according to the principle of microscopic reversibility the overall rate equation has the form:

$$Rate = (k_1 a_{H^+} + k_2 a_{H2CO3^*} + k_3 a_{H2O})(1 - \frac{a_{Ca^{2+}} a_{CO_3^{2-}}}{K_{sp}}) \quad (8)$$

where k_1, k_2, and k_3 are reaction rate constants for the different pathways [mol m^{-2} s^{-1}]; a_{H+}, a_{H2CO3*}, a_{H2O}, a_{Ca+2}, and a_{CO3-2} are the activities of the respective species [-]; and K_{sp} is the equilibrium constant [-]. From equation 8 it is clear how rate would respond under various conditions. At low pH and low pCO_2 the first reaction dominates, also because the rate constant is several orders of magnitude larger. At higher pH and high pCO_2 then the second reaction becomes dominant due to the increased dissolved CO_2 (since H_2CO_3* = CO_2 + H_2CO_3). Close to equilibrium, so high pH, the reaction starts to become controlled by the third reaction due to the lack of hydrogen ions and carbonic acid and the presence of carbonate. However, Peng et al. (2015) have shown the importance of the second reaction when simulating conditions of CO_2-sequestration, specifically very high pressure (~10 MPa) and therefore pCO_2. This stimulates the second reaction immensely and as such should not be omitted from calcite rate expressions, which often is done. Another interesting observation is the apparent feedback at high pCO_2, namely that according to R2 bicarbonate is released, which at the low pH experienced at high pCO_2 would result in the formation of H_2CO_3 due to the carbonate speciation. This would essentially inhibit R1 through the consumption of H^+ ions and further stimulate R2.

Table 1 *Reaction rate constants and equilibrium constant for calcite dissolution/precipitation pathways at T=25ºC, from Chou et al. (1989), and equilibrium constant is from Plummer and Busenberg (1982). Activation energies are from Plummer et al. (1978) and are used to determine the rate constants at T=50ºC.*

Reaction	Rate constant [mol m^{-2} s^{-1}]	Equilibrium constant [-]	Activation Energy [kJ/mol]
R1	0.89	-	8.37
R2	$5.01 \cdot 10^{-4}$	-	41.88
R3	$6.6 \cdot 10^{-7}$	$10^{-8.48}$	33.08

Other aqueous reactions that are of importance to the system are the carbonate speciation reactions, with associated equilibrium constants (Koutsoukos and Kontoyannis, 1984):

$$HCO_3^- \leftrightarrow H^+ + CO_3^- \quad \text{with } K_1 = 4.446 \cdot 10^{-7} \quad (R4)$$

$$H_2CO_3^* \leftrightarrow H^+ + HCO_3^- \quad \text{with } K_2 = 4.688 \cdot 10^{-11} \quad (R5)$$

2.4 Mass Transport Limitations

Equation 8 and the corresponding rate constants are determined from laboratory measurements, in which solutions are generally well-mixed. However, there often appears to be a discrepancy between rates measured in the field and those measured in the lab (Li et al., 2006). This is because the well-mixed assumption does not always apply in reactive flow in porous media, let alone at field-scale. In fact, even in lab experiments Pokrovsky et al. (2005) showed that gradients can occur at relatively fast rotation speeds when using the rotating disc technique, leading to lower observed rates. The reason for the discrepancies is due to issues of scale at two scales: first is heterogeneity in porous media at the Darcy to field scale (Li et al., 2006; Li et al., 2007), and second is concentration gradients within individual pores (Li et al., 2008). Essentially, the problem from both arises from the distribution of reactant (or product) in the modelled domain: assuming a well-mixed system implies that all the reactant is available for reaction at all the reactive mineral surfaces, which leads to overestimations of the rate. Fredd and Fogler (1998b) also showed that for calcite dissolution in a weak acid (acetic acid) at low pH (<~2.9) the rate of reaction was dependent on both the transport of reactants to the surface and products away from the surface (Fig. 4). They report that both limitations limit the reaction considerably more than either limitation alone.

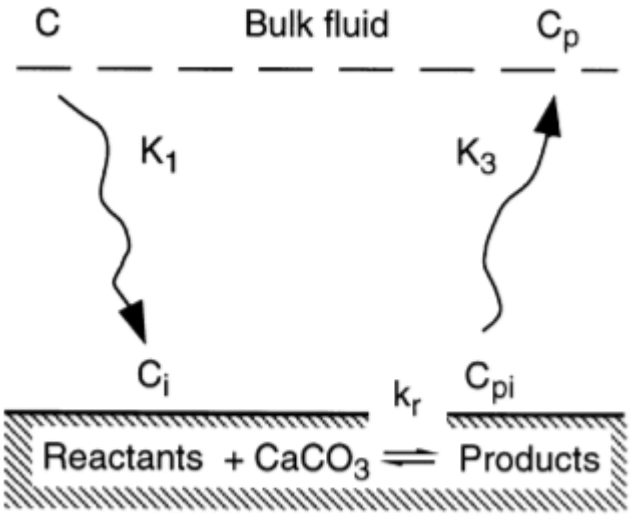

Figure 4 *Schematic of dissolution model used in Fredd and Fogler (1998b) accounting for transport limitation for reversible surface reactions. K_1 and K_2 are the mass-transfer coefficients of reactants and products, respectively, to and from the surface as determined from Levich (1962), and k_r is the reaction rate constant. Image from Fredd and Fogler (1998b).*

Implementation of mass transport limitations on reaction rates can be done in a couple ways. One method which is often employed in chemical engineering is the use of dimensionless mass-transfer coefficients like the Sherwood number (e.g. Panga et al., 2005; Kalia and Balakotaiah, 2007). Another method that was used by Fredd and Fogler (1998a) was by using the dissolution model schematically shown in figure 4 and a solution for convective-diffusive laminar flow in a pipe which gave the average mass transfer along the length of the pipe (Levich, 1962). Another interesting approach was that of Wolterbeek and Raoof (2018) who devised a rate of reaction based on the rate of diffusion under the assumption of steady state. The interesting part about their approach was that the rate was defined as either mass-transfer limiting or reaction-rate limiting, depending on which rate is in fact limiting at the time. A similar approach will be employed in this research but differs due to increased complexity of the chemical system.

2.5 Optimum Injection Rate and Damköhler Number

The optimum injection rate alluded to in previous sections is a well-documented phenomenon. The idea centres around the least amount of acid required to get a desired permeability (e.g. K/K_0=100). This amount of acid is defined as the number of pore-volumes to breakthrough (PVBT), and is determined at the point when the network permeability has increased by a factor of 100 (e.g. Fredd and Fogler, 1998a; Panga et al., 2005). Fredd and Fogler (1998a) discovered that for different acids the optimum injection rate would change (Fig. 5a), with acids with a lower effective diffusion coefficient having a lower optimum but a higher PVBT. This indicates there may be a relationship between the reactivity of the system and the advective-diffusive transport. Figure 5b shows the PVBT curves plotted against the inverse of the Damköhler number, which is a dimensionless number relating the reactivity of the system to advection (Eq. 9). The graph shows that there exists an optimum Damköhler number which is the same for all acids. In their analysis they defined the Damköhler number based on the dissolution model shown in figure 4, and has the form:

$$D_{a,Fredd} = \frac{4 \cdot l \cdot k_{eff}}{d \cdot u} \tag{9}$$

where l is the representative length of the wormhole [L], k_{eff} is the effective rate constant [L T^{-1}], d is the wormhole diameter [L], and u is the superficial fluid velocity [L T^{-1}]. Other forms of the Damköhler number were also used but were not able to represent the reactivity accurately and so were not able to reproduce figure 5b. However, due to the difference in the dissolution model used in this study **Eq. 9** is not applicable, and so in this paper the Damköhler number is defined in a more general form:

$$D_a = \frac{R \cdot L}{C_a \cdot u} \tag{10}$$

where R is the average rate of reaction over the whole simulation [M T^{-1}], L is the length of core [L], C_a is the inlet acid concentration [M L^{-3}], and u is the fluid velocity [L T^{-1}]. In our simulations, because we define two reaction pathways, and thus two acids (i.e. H^+ and $H_2CO_3^*$), the inlet acid concentration was defined as the sum of the two concentrations:

$$C_a = C_{H+} + C_{H2CO3^*} \tag{11}$$

As the Damköhler number is defined in equation 10, it is essentially the ratio of the rate of acid consumption and rate of acid transport. Normally, there should be a stoichiometric coefficient in the numerator, but since the stoichiometry for each pathway is 1:1 it is not necessary here. The main difference between this definition of the Damköhler number and those reported in other papers, and to a certain extent equation 9, is that equation 11 does not assume the effective average rate of reaction but rather determines it after the fact (i.e. *a posteriori*). Equation 9 is also dependent on simulation results in that it is dependent on the dimensions of the wormhole to determine the effective reaction constant through the incorporation of mass-transfer in their dissolution model, and so effectively determine the Damköhler number in the wormhole. However, this method still assumes the effective rate of reaction is based solely effective reaction constant. Nevertheless, equation 9 has shown to accurately represent the ratio of reactivity and transport, for both experiments (Fig. 5) and numerical experiments.

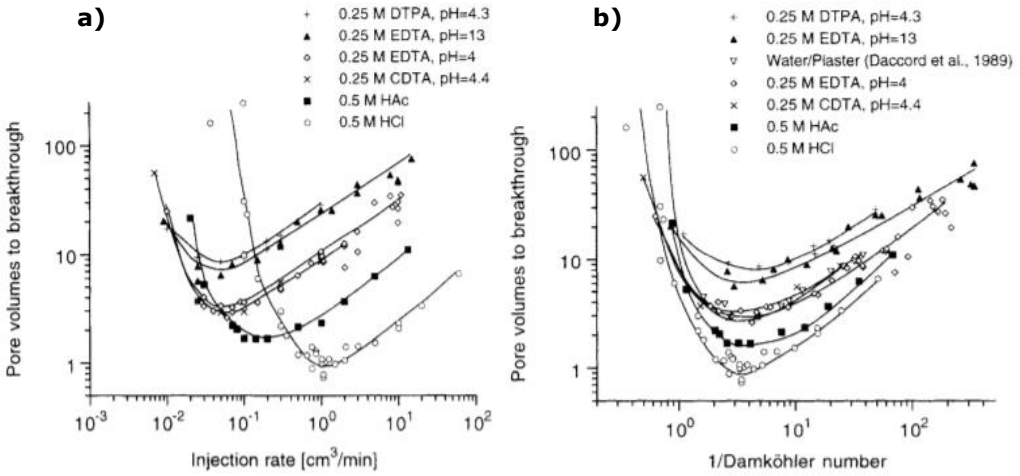

Figure 5 *Plots of PVBT vs (a) injection rate and (b) inverse of Damköhler number. 5b also includes data from Daccord et al. (1989) which was water/plaster system. Shows the relationship between the optimum injection rate based on the reactivity of the system. Image from Fredd and Fogler (1998a).*

Another interesting aspect of modelling wormhole formation is the effect of boundary conditions. Cohen et al. (2008) looked at wormholing for a variety of different domains, from 'confined' to 'unconfined', and found that 'confined' domains generally overestimated the optimum injection velocity. Furthermore, they report a much wider range of injection velocities that are in the dominant wormhole regime than shown in figure 5, and that the difference between the two types of domains is accentuated at the lower velocities.

3 Methods

In this section the methodology of the coupling is discussed, as well as the generated pore-network and PHREEQC model characteristics, and a description of the developed rate expression to account for mass-transfer limitations. Finally, a brief overview of the different simulation conditions will be given.

3.1 Coupling Procedure

The coupling of PHREEQC and PoreFlow is done within a BATCH executable, which can be found in Appendix A1. A flowchart representing the coupling of PoreFlow and PHREEQC is shown in figure 7. Essentially, the 3D network generated in PoreFlow is represented in a 1D domain described in PHREEQC (Fig. 6). The domain in PHREEQC is discretized into several cells that map the 3D network, and PoreFlow calculates the reactive surface area for all pore throats within the corresponding segment in the 3D network. PHREEQC then calculates the amount of kinetically dissolved calcite during reactive transport and transfers that information to PoreFlow for the throats to become larger or smaller. One limitation of this is that it is not able to capture heterogeneities within a given segment (e.g. Li et al., 2006), and as such if PHREEQC calculates net dissolution for a given cell then dissolution is determined for all throats in PoreFlow, when in reality it is possible that some throats may experience precipitation. This issue is not addressed in this study, and it is assumed to be negligible. However, possible solutions will be discussed in the description of dissolved/precipitated calcite distribution in PoreFlow.

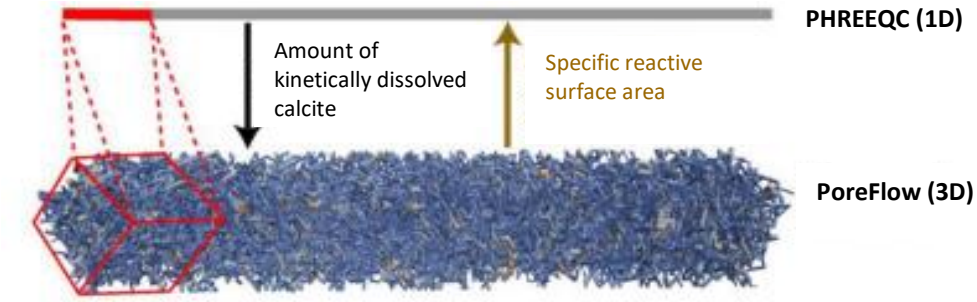

Figure 6 *Schematic diagram of coupling between PHREEQC and PoreFlow. PoreFlow determines the specific surface area of a segment, and PHREEQC uses that information to calculate reactive transport for certain number of timesteps. The amount of dissolved/precipitated calcite is distributed in PoreFlow among the throats for the corresponding cells. Image modified from Ameri et al. (2017).*

As stated previously, transport is calculated in PHREEQC by equation 5, and doesn't rely on PoreFlow for any changes in flow. The main uncertainty associated with this is the applicability of the ADR equation in the presence of wormholes due to the possibility of non-Fickian flow. However, it should be noted that Zheng et al. (2019) were able to accurately model non-Fickian transport through rough fractures using the local advection-dispersion equation and Taylor dispersion coefficients.

PHREEQC requires the specific reactive surface area for each cell (in *PHREEQC_CELL_INFO.TXT*) as input, and PoreFlow requires the amount of change of calcite (in *del_Calcite.txt*). Thus, PoreFlow is initially run with a *del_Calcite.txt* that is full of zeroes (Fig. 7) to determine the initial reactive surface area, and afterwards PHREEQC can be run. To reduce computational cost the coupling between the two programs is not done at every time-step. Instead, within the PHREEQC model transport and reaction are calculated for several time-steps before transmitting the information back to PoreFlow, as such a single loop shown in figure 7 will include several time-steps. The assumption with this is that the amount of dissolved calcite will negligibly change the reactive surface area under a certain time-step. The number of time-steps done in PHREEQC is dependent on the flow regime and the reactivity of the system. Within the PHREEQC model an initial solution is determined for the infilling solution (CO_2-saturated water with a pCO_2 of 10 MPa) and the resident formation water (water in equilibrium with calcite). Furthermore, the porous media is assumed to be wholly made of calcite. After reaction and transport, the new solution compositions and remaining amount of calcite for each cell are outputted to be used as input for the subsequent PHREEQC run. Once the desired number of loops has been reached, the model ceases. For more details on main executable that couples the two programs and the main PHREEQC input file along with other relevant input files the reader is referred to the Appendix.

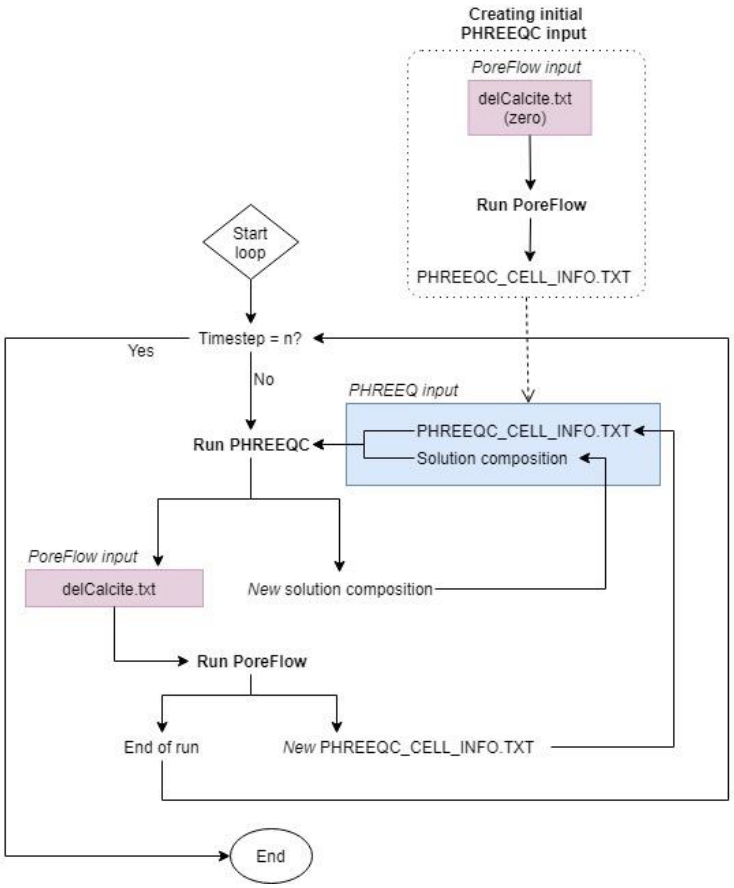

Figure 7 *Flowchart representing the coupling process. As input PHREEQC requires from PoreFlow the file PHREEQC_CELL_INFO.TXT, which contains the specific surface area for each cell. PoreFlow requires from PHREQC del_Calcite.txt, which contains the change in calcite in number of moles. Important to note is that within a single PHREEQC run several time-steps are evaluated to reduce computational demand.*

The distribution of calcite within PoreFlow is done only in the throats. The reason for this is because it is only the throats which inhibit flow and thus determine the permeability. To account for the friction of pore bodies and the thus the contribution to resistance to flow, the throat lengths are artificially increased when the network is generated (Eq. 2). The weighting of each throat for the distribution of calcite is dependent on the inverse of the resident time of each throat, given by:

$$W_{ij} = \frac{\frac{1}{T_{ij}}}{\sum \frac{1}{T}} \tag{12}$$

where W_{ij} is the weighting for throat *ij*, T_{ij} is the residence time [T] of throat *ij*, and the denominator is the sum of all inverse residence times. The idea is that if the if a throat has a low residence time then it more reactants flow through it and thus dissolves more calcite. Inversely, if the residence time is low then it is exposed to less 'new' fluid and thus the solution will be closer to equilibrium. However, this weighting scheme can be modified to account for other factors that may be important. For example, it could include a term for the volume of the throat since it can be argued that the larger the volume the greater the capacity to dissolve. Or a term for its x-position could be incorporated to account for distance from the inletting pores (with flow in the x-direction). This weighting scheme could also include an algorithm that can better deal with the issues of heterogeneity discussed previously such that it can also allow for precipitation in certain throats under certain conditions even if the net rate shows dissolution. However, this lies outside the scope of this work and is relegated to future research.

Once the weighting is determined for each throat, the amount of calcite (in moles) removed from each throat is determined. The number moles is converted to a volume change using the molar mass and

density of calcite: 100.0869 g/mol and 2.711 g/cm^3, respectively. The new radius of the throat and the change in radius can then be determined with:

$$R_{ij,new} = \sqrt{R_{ij}^2 + \frac{dV_{ij}}{\pi \cdot L_{ij}}} \quad (13)$$

$$dR = \sqrt{R_{ij}^2 + \frac{dV_{ij}}{\pi \cdot L_{ij}}} - R_{ij} \quad (14)$$

where $R_{ij,new}$ is the new radius [L] of throat *ij*, R_{ij} is the current radius [L] of throat *ij*, *dR* is the change in radius [L], dV_{ij} is the change in volume [L^3] for throat *ij*, and L_{ij} is the length [L] of throat *ij*.

3.2 Model Characteristics

3.2.1 Pore-Network

The pore-network generated was based on network characteristics for Indiana limestone reported in Freire-Gormaly et al. (2015) and Gharbi and Blunt (2012). Both studies used the maximal sphere method on the processed micro-CT images to determine the pore-network. In this study, the mean pore-radius from Freire-Gormaly et al. (2015) was used to determine the pore-size distribution, and the mean coordination number was taken from Gharbi and Blunt (2012). With these two parameters the network was generated, with the network characteristics shown in table 2. The distributions for the pore body radius and throat radius can be found in Appendix A5. The average throat radius is slightly lower than reported in Freire-Gormaly et al. (2015), which was ~22um, and the permeability is around 3.5 times smaller than what was reported in Gharbi and Blunt (2012). The dimensions of the network are N_i=N_j=15, and N_k=200, with the lattice distance being 160 um. This lattice distance was chosen such that the porosity would be ~13%, similar to the porosity reported in the aforementioned studies. Note that the average throat length deviates significantly from the lattice distance. This is due to the enhancing of the throats mentioned earlier, which artificially lengthens throats to account for the friction of the pore bodies. The final network can be seen in figure 8.

Table 2 *Characteristics of the generated pore-network. The number of pore bodies and throats are for the network after the elimination procedure.*

# of pores	32159
# of throats	51732
Average coordination number	3
Average pore radius [um]	32.4
Max pore radius [um]	109.92
Average throat radius [um]	15.3
Max throat radius [um]	60.32
Average throat length [um]	268.7
Max throat length [um]	2785.56
Porosity [%]	~13.3
Permeability [m^2]	1.52E-12

Table 3 *Properties of each cell in PHREEQC. Note that the porosity and amount of calcite are only the initial quantities; as dissolution occurs they increase and decrease, respectively.*

Length [mm]	1.6
Calcite [mol]	176.85
Volume water [L]	1
Porosity [%]	~13.3
Dispersivity [mm]	0.16

3.2.2 PHREEQC Domain

The 1D PHREEQC domain consists of 20 cells, with each cell having the same initial porosity as the porosity for the whole network (Table 2). Furthermore, the initial amount of calcite available for reaction in each cell was determined by dividing the volume of water in each cell (1L) by the initial porosity and using the density and molar mass of calcite to get the number of moles. A summary of the properties of each cell is given in table 3. The pore-network and corresponding PHREEQC cells mapped onto the network are shown in figure 8.

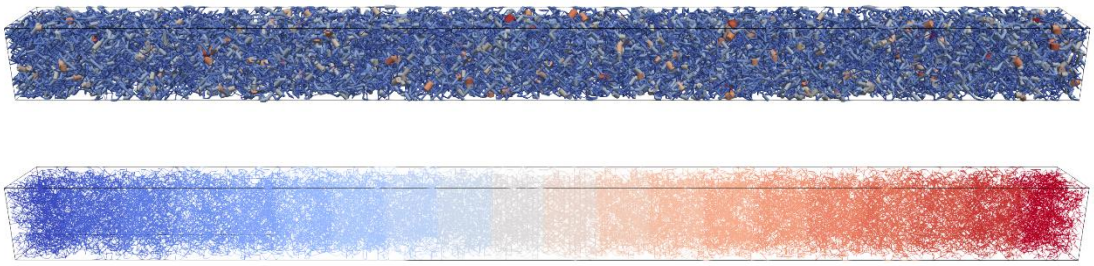

Figure 8 *The generated pore-network used as input for the simulations (top), showing the pore throats scaled to the respective radii. Bottom image shows the pore-network with the colour scheme indicating the respective PHREEQC cells: you can faintly distinguish the lines in between the colours indicating the boundaries of the PHREEQC cells.*

3.3 Rate Expressions

In this section the rate expressions used in the various simulations are given. For simulations not considering mass-transfer limitations equation 8 is used to determine the overall rate in each cell. As for the rate expression that accounts for mass-transfer limitations, the dissolution model relies on a couple of assumptions. Firstly, it is assumed that the system is locally at steady state, which allows for balancing of the flux of diffusion to and from the surface of a given species and the rate of consumption/production of that species at the surface. It is believed that this assumption is valid relatively soon after initial contact between the acid and calcite and so can be used, however this is not substantiated. Secondly, it is assumed that under mass-transfer limiting conditions the surface speciation is in equilibrium, such that the rate of diffusion to or from the surface has as boundary concentrations the bulk concentration and equilibrium concentration. While this is an extreme case of mass-transfer limitation, it can help build some perspective when comparing to a reaction-limited reaction (Eq. 8), which is also an extreme. Thirdly, it is assumed that reactions in each cell in PHREEQC can be viewed as occurring within a tube with the same radius as the average throat radius of throats in that cell. This assumption helps with selecting an appropriate diffusion model and is believed to have credence since throats in PoreFlow are also tubular. The fourth assumption is that the average concentration within the tube is at half of the radius. This is based on the work of Raoof and Hassanizadeh (2010) on modelling adsorbing solutes in a tube, who found that the average concentration was at half of the pore radius. However, it should be noted that the system in this study is more complex with speciation reactions occurring throughout the pore-space. Nevertheless, it is believed that this assumption is applicable for Ca^{2+} within the pore. With these four assumptions we can already formulate the rate expression using the solution for steady-state diffusion in a hollow cylinder from Crank et al. (1975), which is:

$$R_{MT-lim} = -D \frac{C_{eq} - C_{bulk}}{\ln(2)} \frac{1}{R} \tag{15}$$

$$R_{eff} = min\{R_{MT-lim}, R_{R-lim}\} \tag{16}$$

where D is diffusion coefficient [L^2 T^{-1}], C_{eq} is the equilibrium concentration [mol L^{-3}] (i.e. surface concentration), C_{bulk} is the bulk concentration [mol L^{-3}] (i.e. cell concentrations calculated by PHREEQC), R is the average pore-throat radius [L], R_{MT-lim} is the rate of the mass-transfer limitation [mol L^{-2} T^{-1}], R_{R-lim} is the rate in equation 8, and R_{eff} is the effective rate [mol L^{-2} T^{-1}]. The derivation for equation 15 is given in the Appendix A6. Now we have an expression that can be evaluated for every cell and at every time in PHREEQC. Furthermore, as with Wolterbeek and Raoof (2018) the rate expression is expressed as the minimum of the two possible limitations. The only element missing now is to select which species will represent the diffusion model. Thus, the fourth assumption is that the gradient in Ca^{2+} concentration is representative of the rate of reaction. Of all the species this is the most logical due to its 1:1 stoichiometric ratio with calcite: for every mole of calcite dissolved one mole of Ca^{2+} is produced. In addition, Ca^{2+} is unaffected by the speciation reactions that affect the other species of

interest, and thus its lateral transport in a pore (assuming laminar flow) can be assumed to be governed by diffusion and reaction alone.

3.4 Simulation Conditions

In this research three sets of simulations will be tested: two in which reaction-limited dissolution is assumed at temperatures of 25ºC and 50ºC, and one including mass-transfer limitations at a temperature of 50ºC. The simulations will henceforth be referred to as R_{lim}-25, R_{lim}-50, and MT_{lim}-50. Each of these systems will be tested for a variety of injection velocities to determine the PVBT curves and will be done with infilling solution at equilibrium with CO_2 at a pressure of 10 MPa, representative of reservoir conditions. The different velocities and frequency of coupling between PHREEQC and PoreFlow for each simulation are shown in table 4. In addition, two more simulations will be done to illustrate that the model acts as expected and will serve as validation cases. The first will be to show that the chemistry of the system works as expected, and the second will be to show that the model can capture the simple case of face-dissolution.

Table 4 *Flow velocities and number of pore volumes run for each simulation. The velocity varies for the different simulation conditions due to different reactivities at the different temperatures and dissolution models. 'dt' denotes the advective time-step in PHREEQC, and '# of shifts' is the number of reactive-transport steps done within PHREEQC before transferring the information to PoreFlow. This number was determined for each velocity such that the overall network porosity would increase by less than 0.5% per loop. For faster flows more shifts can be done since less calcite dissolves for the smaller time-steps. 'PV' denotes pore volume, and '# of Loops' is the number of times PHREEQC and PoreFlow are run together (i.e. full cycle in Fig. 7). The 'Pore Volumes' column shows the total number of pore volumes run for each simulation.*

Simulation #	*Velocity [m/s]*	*dt [s]*	*# of Shifts*	*# of PVs per loop*	*# of Loops*	*Pore Volumes*
R_{lim}-25						
1	8.00E-03	0.2	150	7.5	226	1695
2	1.60E-02	0.1	200	10	150	1500
3	3.20E-02	0.05	350	17.5	300	5250
4	8.00E-02	0.02	600	30	200	6000
5	1.60E-01	0.01	1000	50	100	5000
6	3.20E-01	0.005	1800	90	100	9000
7	8.00E-01	0.002	3000	150	100	15000
8	1.60E+00	0.001	6000	300	75	22500
R_{lim}-50						
1	1.07E-02	0.15	150	7.5	999	7492.5
2	1.60E-02	0.1	150	7.5	280	2100
3	3.20E-02	0.05	200	10	180	1800
4	8.00E-02	0.02	400	20	80	1600
5	1.60E-01	0.01	500	25	80	2000
6	3.20E-01	0.005	1000	50	50	2500
7	8.00E-01	0.002	2000	100	50	5000
8	1.60E+00	0.001	4000	200	50	10000
MT_{lim}-50						
1	3.20E-06	500	125	6.25	324	2025
2	8.00E-06	200	100	5	600	3000
3	3.20E-05	50	300	15	145	2175
4	8.00E-05	20	400	20	120	2400
5	1.60E-04	10	500	25	150	3750
6	3.20E-04	5	1000	50	100	5000
7	8.00E-04	2	2500	125	100	12500
8	1.60E-03	1	4000	200	120	24000

4 Results

4.1 Model Behaviour

To test whether the chemistry of the model works as expected, a simulation was run in which each PHREEQC cell had an initial amount of calcite of 0.04 moles, with cell velocities of 3.2 mm/s (time-step = 0.5s) and at a temperature of 25ºC. Figure 9 shows the pH (circles) and amount of calcite (crosses) in each cell after 0.5 pore volumes, and lines to indicate the equilibrium pH for different systems. The bottom horizontal line (yellow) is the equilibrium pH for a CO_2-water system (pH=~3) and shows that once the calcite in a cell is completely reacted the pH becomes that of the injected solution. The top horizontal line (black) is the equilibrium pH for a calcite-water system (pH=~10) and shows that the CO_2 saturated water has not yet reached cells 17-20. The middle line (red) signifies the equilibrium pH for a CO_2-calcite-system, and the graph indicates that when the infilling solution comes in contact with the calcite (i.e. cell 6 in figure 9) the reaction is so fast that nearly all the acid is consumed to close to the equilibrium condition, which is expected for the fast reaction of calcite dissolution. The three plateaus illustrated in figure 9 demonstrate that the chemistry of the model works as expected.

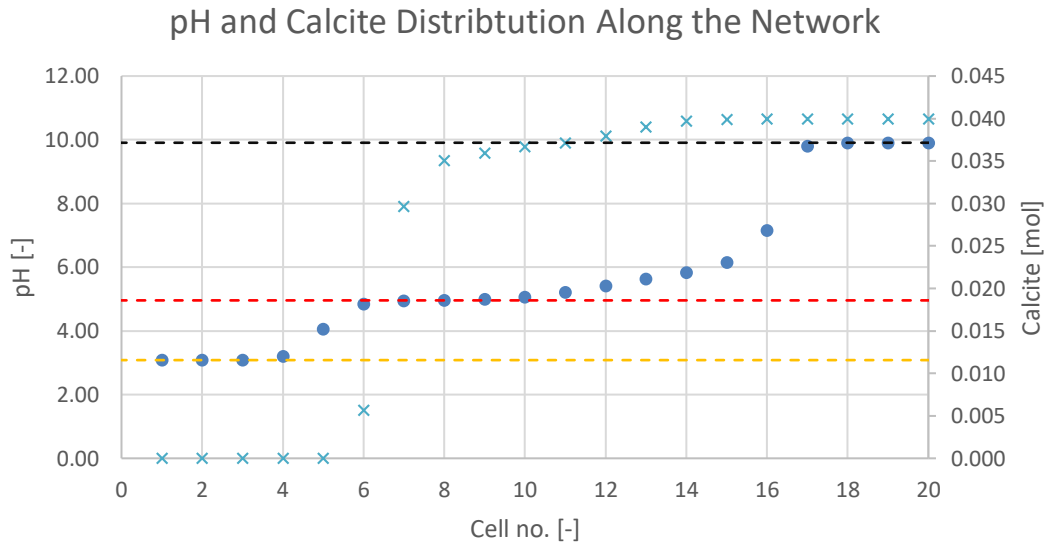

Figure 9 *The graph shows the pH (circles) and amount of calcite (crosses) [mol] per cell after 0.5 pore volumes, with an initial amount of calcite of 0.04 mol per cell and at a temperature of 25ºC. The velocity in each cell was 3.2 mm/s. The dashed lines represent the equilibrium pH for different systems: CO_2-calcite-water (red, middle), CO_2-water (yellow, bottom), and calcite-water (black, top).*

Figure 10 *The pore-network displaying throats experiencing dissolution after 5 pore volumes for flow velocity of 0.32 mm/s. The image shows that for the case of slow flow the dissolution pattern exhibits face dissolution. The quantities displayed in the legend are in um.*

The simulating of face dissolution is done by having a low velocity of 0.32 mm/s (time-step = 5s), such that only the first cell in PHREEQC should have dissolution. This should translate to only the throats in the beginning of the network displaying a change in throat radius, which is illustrated in figure 10. The figure shows the change in pipe (i.e. throat) radius after 5 pore-volumes, indicating that dissolution occurs solely at the inlet of the network. Naturally, since PoreFlow distributes the dissolved calcite over all the throats in a cell, the extent of the dissolution front is dependent on how many 1D cells are defined in PHREEQC: a larger number of cells would more accurately represent the extension of the dissolution. Nevertheless, figure 10 shows that face dissolution can be modelled and suggests that the coupling of the models works as expected.

4.2 Simulation Results

The first set of results that will be shown is the permeability response to the acid injection, under the same conditions (i.e. temperature) and varying velocities (figure 11). For the sake of clarity, not all permeability curves for all the simulated velocities are shown. Figure 11 shows a typical response for permeability evolution for varying velocities, with very slow and fast flows reaching a given permeability after more pore-volumes than intermediate flow speeds. The simulations shown in figure 11 are for the system at 25°C (R_{lim}-25), and the optimum velocity being 0.032 m/s since at that velocity the fewest number of pore-volumes is necessary to achieve 100 times increase in network permeability (i.e. lowest PVBT). Another way to represent this information is to plot the PVBT against the velocity (figure 12), which better illustrates the optimum condition, indicated by the minimum in the curve. Unfortunately, the model was unable to simulate slower velocities because at a certain point PoreFlow would crash, likely due to pressure solver being unable to converge due to pore throat radii having increased too much. When compared to figure 5, it is clear that the trend is quite similar, with the main difference being the magnitude of the optimum velocity and the magnitudes of the PVBT. The vertical lines in figure 12 indicate the regime where a dominant wormhole (Fig. 1) is expected to occur. As reported in literature, as the velocity increases the dissolution pattern is expected to become more ramified, eventually ending with uniform dissolution. Inversely, as the velocity decreases the dissolution pattern is expected show a conical wormhole, ending with the other extreme of face dissolution.

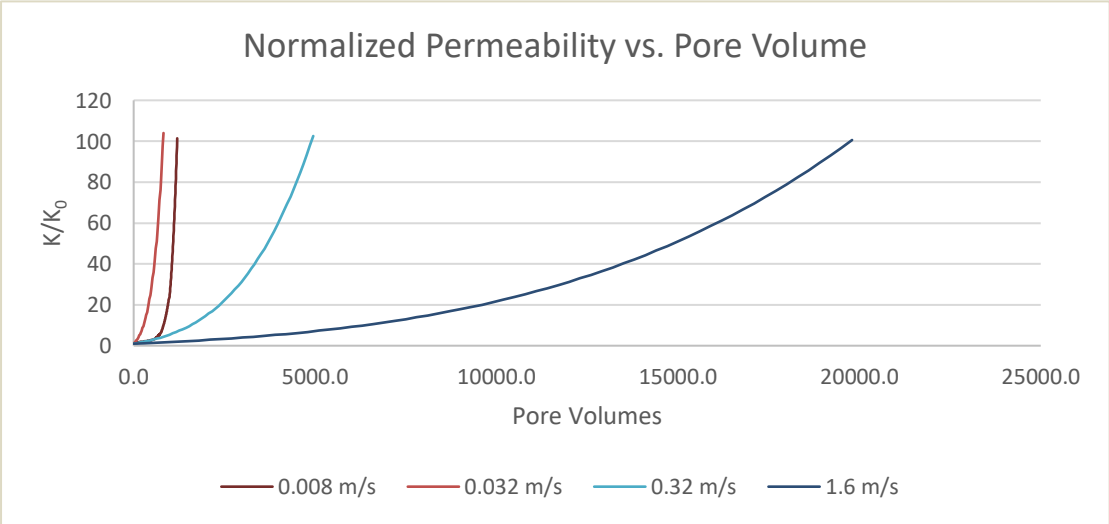

Figure 11 *Evolution of (normalized) permeability for R_{lim}-25 for four selected velocities. The curves stop when the permeability has increased by a factor of 100, defined as the moment of breakthrough. The graph indicates that the optimum velocity to achieve breakthrough is 0.032 m/s as it requires the least number of pore-volumes to do so.*

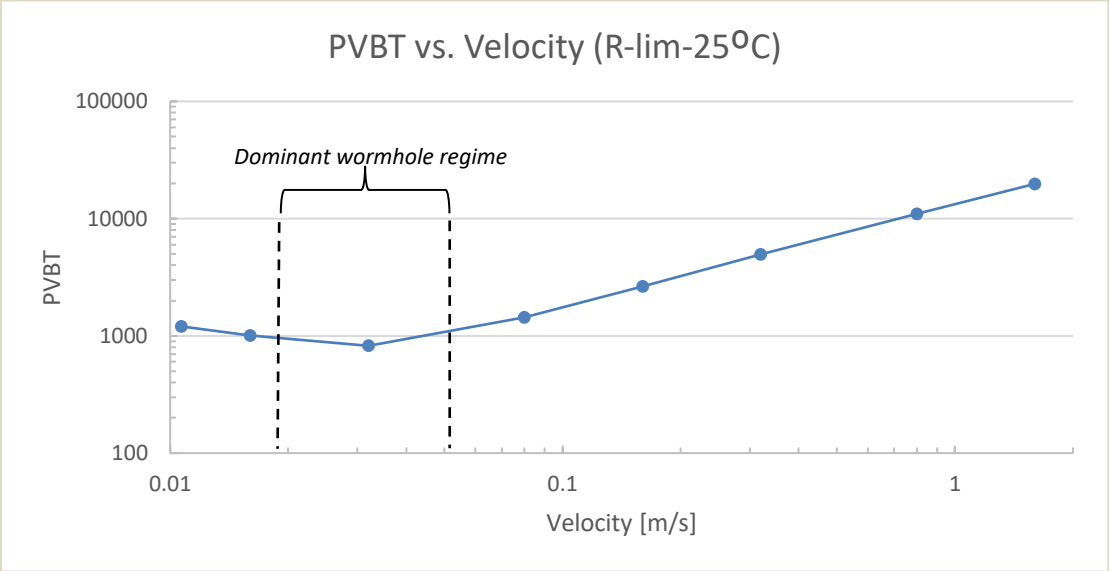

Figure 12 *PVBT plotted against velocity for simulations of R_{lim}-25. Curve indicates a minimum at v=0.032 m/s, which signifies the optimum velocity as the PVBT is minimized. The vertical lines indicate the approximate regime where a dominant wormhole is expected to exist.*

This trend of the PVBT vs. velocity curves having a minimum is apparent for all simulation conditions (Fig. 13). Figure 13 shows the PVBT for all velocities for all simulation conditions, along with both experimental and modelled data from Fredd and Fogler (1998a). As can be seen, there is quite a wide range of optimum velocities and minimum PVBT, with the all the simulations in this research having significantly higher PVBT than those from Fredd and Fogler (1998a). Notably, the optimum velocity for the simulations accounting for mass-transfer limitations (red line with boxes) is significantly lower than for the simulations assuming reaction-limited kinetics. The velocity ranges for MT_{lim}-50 are thus of a similar order to the velocity ranges from the linear coreflood experiments (orange circles). Another interesting observation is the slightly lower minimum PVBT for R_{lim}-25 than for the other two simulations.

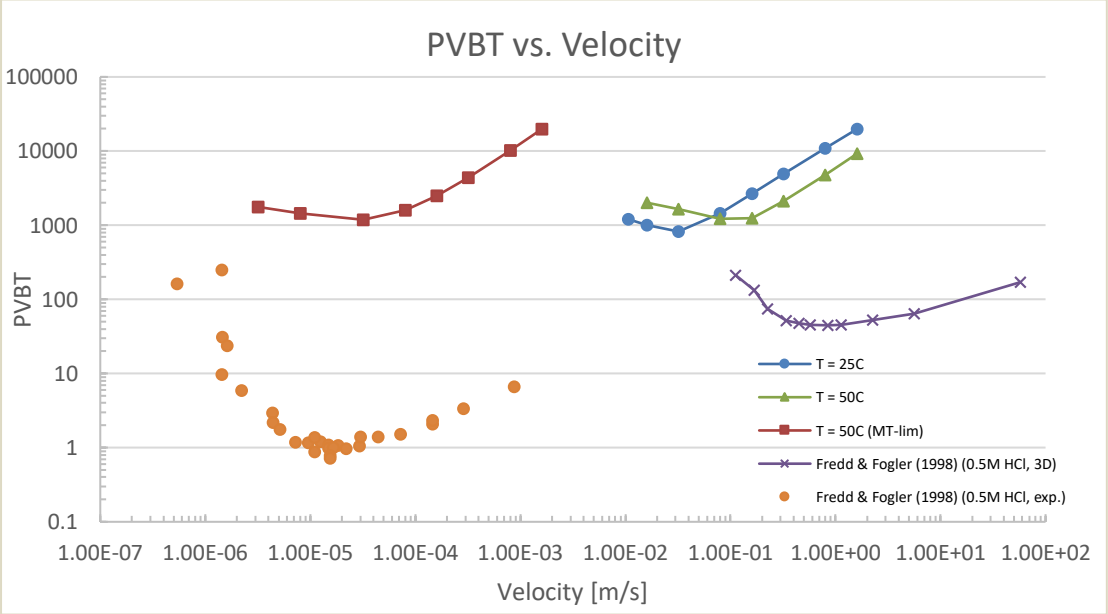

Figure 13 *PVBT vs. velocity for all simulations, including data from Fredd and Fogler (1998a): orange circles are from linear coreflood experiments using limestone cores and injecting 0.5M HCl, and the purple line with crosses is from simulations done using a representative pore-network of a bed of calcite spheres with 0.5M HCL being injected. All curves show the existence of a minimum PVBT, and thus optimum velocity.*

Interestingly, when the PVBT is plotted against the inverse of Damköhler number as defined by equation 10, the data all coincide with each other (Fig. 14), indicating an optimum Damköhler number. This shows that this definition of the Damköhler number accurately describes the system, regardless of temperature or whether systems are defined as reaction-limited or mass-transfer limited. The optimum Damköhler number for the modelled simulations is ~2.2e-2, around a factor 10 smaller than the optimum reported in Fredd and Fogler (1998a) for their experiments (Fig. 5).

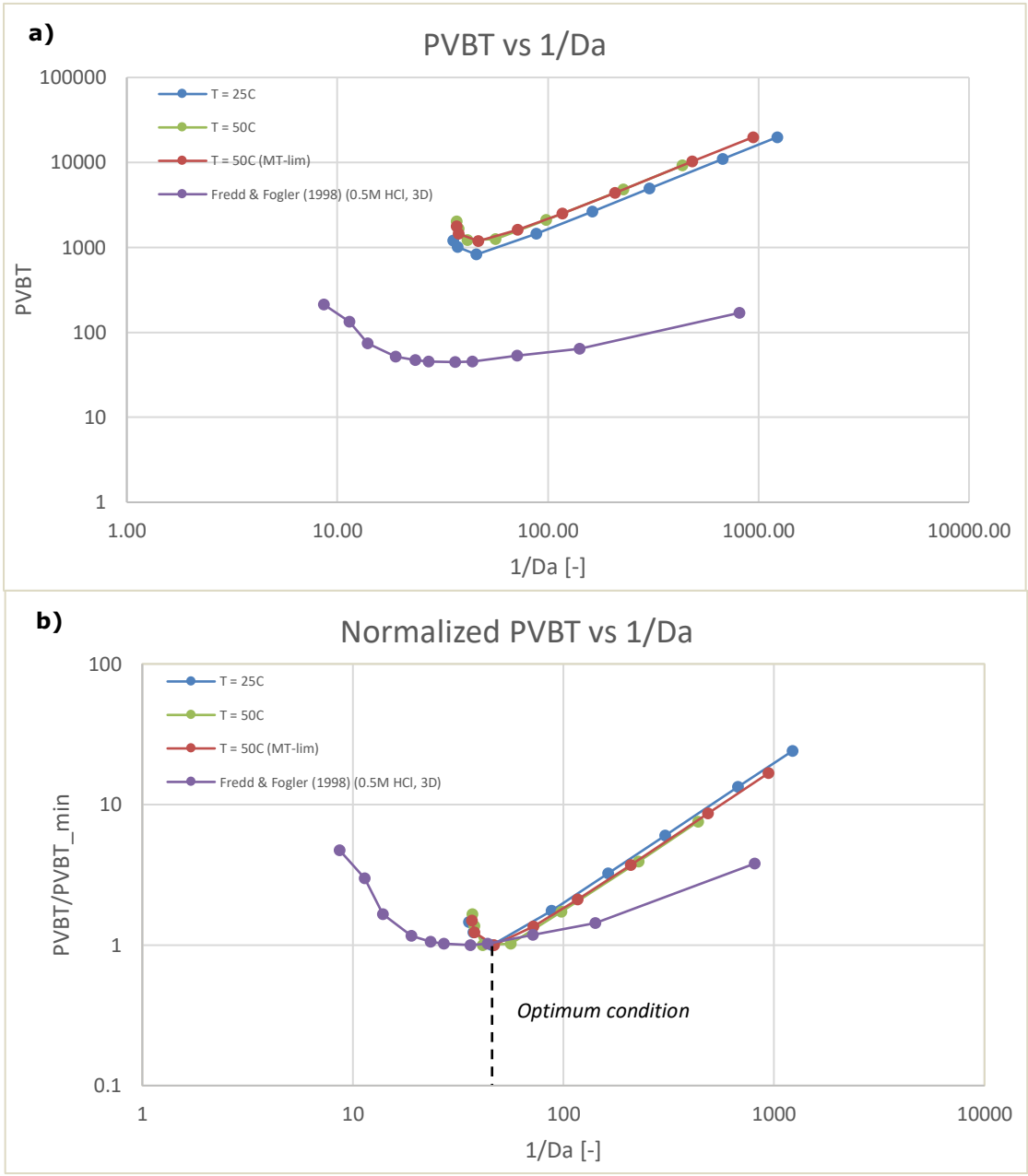

Figure 14 *PVBT plotted against the inverse of the Damköhler number (a) and normalized PVBT plotted against inverse of Da (b). The PVBT are normalized in b) to better illustrate the optimum Da, denoted by the black dashed line. The optimum Da is the same for all simulation conditions, and similar to the optimum of the 3D simulations reported in Fredd and Fogler (1998a).*

Figure 14b plots the normalized PVBT against the inverse Da, better illustrating the optimum conditions for the various systems. While the optimum Da was found to be ~10 times smaller than for the experiments conducted by Fredd and Fogler (1998a), it matches closely with their 3D simulations. However, it should be noted that their Da was calculated in a different way (Eq. 9) to the one used in this study (Eq. 10). Another point of comparison is the trend of the curve as velocity (and thus inverse of Da) increases past the optimum: the slope for the simulations of this research are steeper than when compared to Fredd and Fogler (1998a).

Another aspect worth investigating is the amount of calcite dissolved to reach the 100-fold increase in permeability. Figure 15 shows the porosity of the network once breakthrough has been achieved vs. the inverse of Da, which is an analogue for the amount of calcite dissolved as each network has the same initial porosity. The graph shows that more calcite is dissolved for slow flows to achieve the same permeability increase, but that interestingly for 1/Da > ~47 the amount of calcite dissolved does not further decrease for increasing velocity. The plateau is at a porosity of ~26%, corresponding to a 13% increase in porosity.

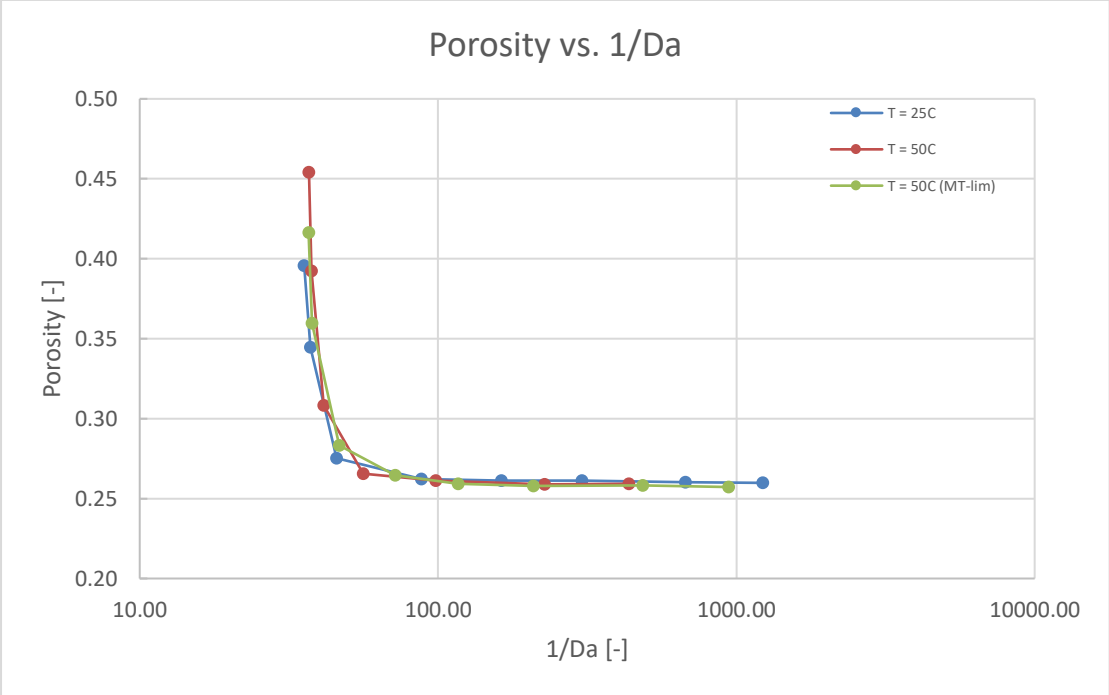

Figure 15 *Final network porosity at time of breakthrough for the different simulations plotted against the inverse of Da. There is an apparent dependency of the porosity evolution on Da, and for velocities greater than the optimum there appears to be little change*

With respect to the dissolution patterns exhibited in the pore-network, the results unfortunately do not show a clear dominant wormhole or any discernible dissolution pattern such as those shown in figure 5. The pore-networks shown in figure 16 are for R_{lim}-25 for the slowest, optimum, and fastest velocities, respectively, at the moment of breakthrough. From these images it can be seen that there is little to distinguish between the networks for the optimum velocity and the fastest flow. The same dissolution pattern is observed for the other simulations (i.e. R_{lim}-50 and MT_{lim}-50) for velocities at or greater than the optimum. The dissolution pattern for the slow flow is quite unexpected, as the size of the throats shown (i.e. radius) is scaled to the discharge through the throats. As such, one would expect the throats in the beginning of the network to be significantly larger than those in the middle and end. Nevertheless, it is believed that this dissolution pattern is simply an artefact of viewing the network in ParaView and does not represent the actual network accurately. In combination with the dissolution patterns, figure 17 shows the effluent pH at the regime of the expected dominant wormhole (i.e. optimum velocity) and shows that the pH decreases slowly as simulation progresses even way past the point of breakthrough (pore volume = ~823). One would expect that once breakthrough has been achieved then the effluent pH would be closer to the inlet pH (~3.1) since flow is focused in the wormhole and thus reacts less, yet this is not observed in figure 17. Reasons for this will be discussed next, along with suggestions for improvement of the model.

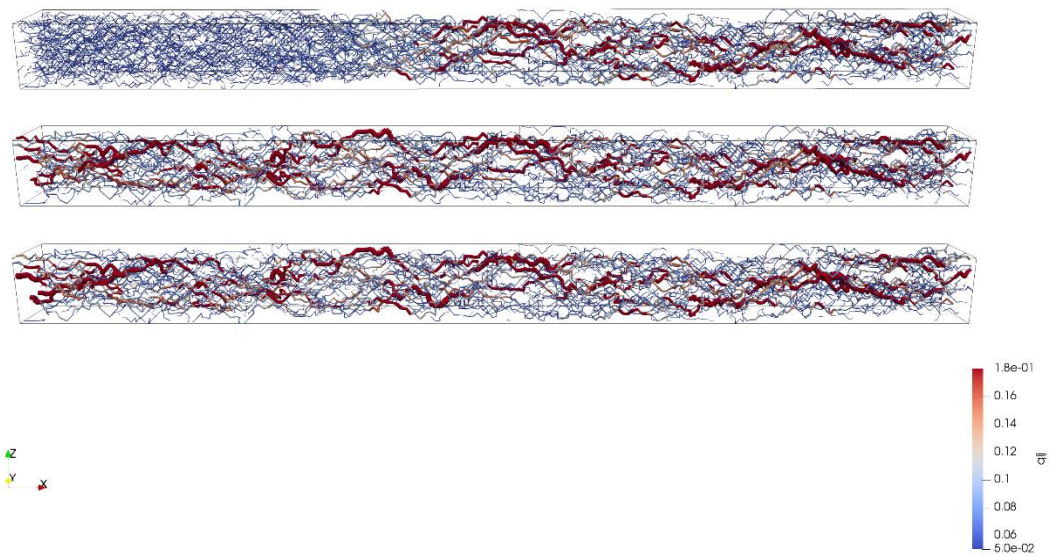

Figure 16 *Pore-networks at moment of breakthrough for three different velocities: slow (top), optimum (middle), and fast (bottom), for R_{lim}-25. The slow and fast flows are the slowest and fastest velocities simulated for R_{lim}-25, respectively. The colouring signifies the magnitude of the flow in the throats, and the size (i.e. radius) of the cylindrical throats is scaled to the discharge through the throat. There is not much difference between the middle and bottom network, and not visible pattern to suggest a dominant wormhole, or other type of wormhole (conical or ramified).*

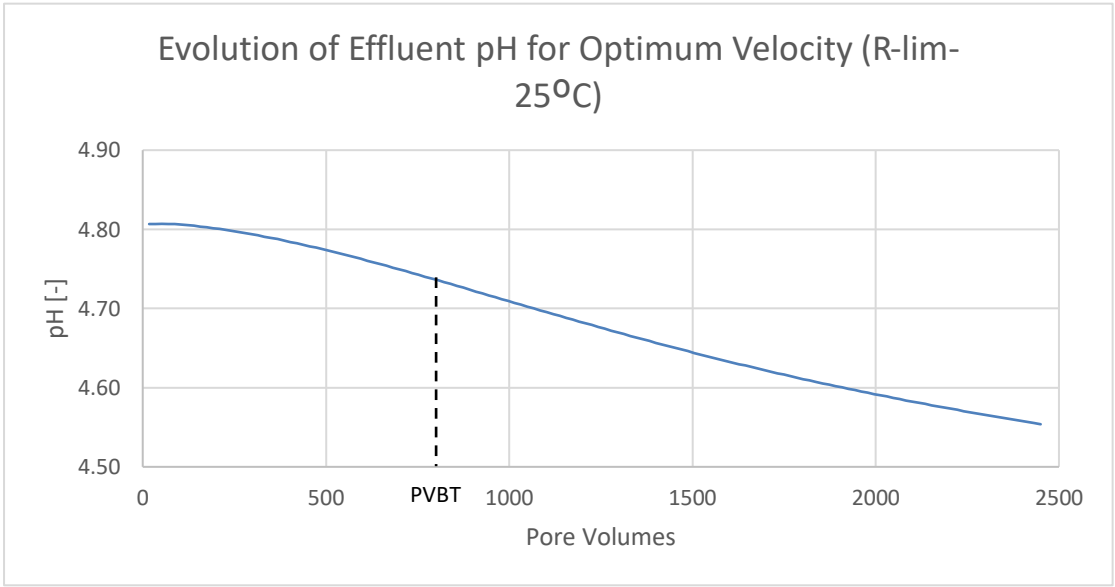

Figure 17 *Evolution of the effluent pH for the optimum velocity simulation for R_{lim}-25. The effluent pH development is shown to almost 2500 pore volumes, which is ~3 times more than the PVBT. The fact that the pH does not drop significantly once breakthrough has been achieved indicates that the coupling does not realistically capture the relationship between the transport and reaction.*

5 Discussion

Following the results, the first point of discussion is the existence of the optimum conditions for the modelled simulations. The optimum condition phenomenon is well-documented and even expected, and thus the fact that the same phenomenon was observed in our simulations despite the absence of any clear/expected dissolution patterns is an indication the existence of the optimum is not solely dependent on the dissolution pattern and the implications they have on transport and reaction, but also the mere balance between reaction and transport. For slow flows, more acid is consumed in the beginning of the network and thus is 'wasted' as it does not contribute much to permeability. On the other hand, fast flows do penetrate the full length of the network, but due to fast flow the amount of time a volume of acid can react is minimal and so in this case acid is also 'wasted'. This spectrum suggests there is a so-called 'sweet-spot' when a volume of acid penetrates the column sufficiently far enough and is simultaneously given enough time react that it is not flushed out, as is evidenced by figures 12-14. Notice that this is independent of the effect a dissolution pattern such as a dominant wormhole would have on the transport of acid: in the presence of a dominant wormhole acid is preferentially transported in the wormhole to the tip where it then reacts and further develops the wormhole. This effect would essentially also decrease the PVBT since a given volume of acid is much more effective in increasing the permeability of the network when reacted at the front of a dominant wormhole than when it isn't necessarily focused in a wormhole. This, among other reasons, is why the PVBT in the simulations of this research are so much higher than those of experiments.

Another interesting observation is the spread of optimum velocities for the different simulations (Fig. 13). In both simulations in which reaction-limited kinetics are assumed, the simulated velocities are several orders of magnitude higher than for the simulations accounting for possible mass-transfer limitations. This makes sense considering the mass-transfer limitations significantly reduce the rate of reaction, so following the previous discussion about wasted acid the velocity must also be several orders of magnitude smaller such that acid is not wasted by simply being flushed through the system before it can react. As a side note, the fact that the range of velocities around the optimum condition for MT_{lim}-50 are of similar magnitude to that of 0.5M HCl in the linear coreflood experiments is at least an indication that the approach to incorporate mass-transfer limitations used gets close to the 'real' rate of reaction in limestone. As for why R_{lim}-25 has a lower minimum PVBT than the other two simulations, an explanation is lacking. On the one hand the lower temperature causes the reactivity of the acids to be lower due the dependence of the reaction constants on the Arrhenius equation. However, on the other hand the lower temperature means more CO_2 is dissolved and the pH is slightly lower, thereby somewhat compensating for the lower reaction constants. As for what effect the reactivity of the system would have on the minimum PVBT is also not very clear, seeing as there is a negligible difference in minimum PVBT for R_{lim}-50 and MT_{lim}-50, but quite a stark difference in reactivity. As such only the general conclusion that the effect of temperature on equilibrium concentrations has an apparent effect on the minimum PVBT can be made.

When the PVBT was plotted against the Damköhler number (Da) as defined by equation 10, the curves seemed to converge, with all sharing the same optimum Da of ~2.2e-2 (Fig. 14). This was also the case for the 3D simulations from Fredd and Fogler (1998a), albeit the Da being defined differently (Eq. 9). This dependency was also found for Fredd and Fogler (1998a) for a variety of systems, but they found different optimum Da for simulations, both 2D and 3D, and experiments. They defined Da using an assumed dissolution model and mass-transfer coefficient for flow in a laminar pipe, which is quite different to how it is defined in this research. Equation 10 doesn't rely on any assumptions regarding reaction mechanisms and limitations, it simply determines the ratio of acid reacted to acid advected. To test the applicability of equation 10 it would ideally be used to calculate the Da for the simulations and experiments reported in the literature, provided enough information, and see if there are any other dependencies of Da that are not accounted for in equation 10 such as dimensions of the domain. Nevertheless, the fact that all the curves aligned in figure 14 show that this model and description of Da was able to reproduce the relationship between PVBT and Da proposed by Fredd and Fogler (1998a), despite the optimum Da being different.

One recurring trend is that the PVBT for all our simulations are significantly higher than those reported in other studies, leading to plots like figure 14b to better illustrate the common dependencies of optimum conditions. This overestimation is common for pore-network models (Panga et al., 2005), and one contributing factor in this case has already been mentioned: the lack of presence of a wormhole leads to permeability being increased less efficiently for a given volume of acid. Another factor is the size of the domain. For cores the pore-volume is relatively large when compared to a pore-network, yet the dimensions of the wormhole do not change much, and thus the amount (i.e. volume) of matrix dissolved is also less relative to the pore volume. Therefore, for larger domains less pore-volumes are necessary to achieve breakthrough, which was also shown in Cohen et al. (2008). Another interesting point which was raised by Gray et al. (2018) is that, at least when comparing to coreflood experiments, there may be discrepancies in the density of the carbonate. In this study the density and molar mass of *pure calcite* was used to determine the associated volume change, but it is not uncommon for density of carbonates to vary. As a result, if the density of carbonate is less than calcite then the associated volume increase would be greater for the same number of moles dissolved, leading to less acid being required to increase permeability.

One new method of analysing the dissolution experiments which may provide some useful information is to investigate the amount of matrix dissolved (i.e. porosity increase) to achieve breakthrough for the different velocities (Fig. 15). Figure 15 shows an interesting trend which is that for velocities ($v \propto 1/D_a$) greater than the optimum the porosity increase at breakthrough, and thus the amount of calcite dissolved, is constant. This would suggest that regardless of whether a dissolution pattern is uniform or shows a dominant wormhole, the amount of porosity increase for each case would result in the same permeability increase. Of course, as will be discussed hereafter, the model developed for this study was unable to show any unique dissolution pattern, except for face dissolution (Section 4.1). However, it would be interesting to see if this relationship would persist in experiments or other simulations in either pore-networks or continuum models in which the distinct dissolution patterns are observed. Furthermore, as was the case with the PVBT and minimum PVBT, the Damköhler number appears to describe the porosity at breakthrough, with there existing a cut-off Da below which (1/Da) the porosity of network at breakthrough does not further decrease. Again, it would be interesting to compare this observation with other results to see if this relationship is unique or not.

Unfortunately, although optimum conditions were found using the developed model, the model was unable to show any dissolution patterns in the wormholing regime (conical to ramified). The networks shown in figure 16 show that for very fast flow and at the optimum velocity the resulting network at breakthrough shows minimal differences, when the latter ideally would have shown a dominant wormhole and the former a more ramified wormhole or even uniform dissolution. The reason why the model is unable to show the different dissolution patterns, except face dissolution, lies in the nature of the coupling. As it is, the entire surface area (as a specific surface area) is given to PHREEQC from PoreFlow, while in reality the effective surface area is dependent on the heterogeneity of the flow. In other words, if the group of throats and bodies in a cell represent a homogeneous medium then each all surface areas count equally. However, if a preferential flow-path begins to form then more acid comes in contact with that surface area, while elsewhere in the cell certain throats will experience very slow flow, and so the effective contribution of those surface areas to the overall rate is less. On the other hand, the redistribution of dissolved calcite will be done based on the relative weightings of the surface area of each throat: if the surface area of a throat contributed more to the rate then it will also receive more dissolution. Of course, coming up with a scheme that accounts for this is quite challenging, but the goal would be that it will allow for the *propagation* of a dissolution front. As it is now, simply distributing the calcite based on the residence time doesn't consider the connectedness of pores and throats, which is essential to the transport of acid and as such essential in modelling the dissolution pattern. This, along with investigating the crashing of PoreFlow for slow velocities, are the most important areas of improvement of this model. Nevertheless, despite the shortcomings the approach seems promising and greatly reduces computational costs when compared to other models. The longest simulation took around 5h (shortest 45min) on a laptop with an Intel I7 7700 HQ processor (quad-core) with a clock-speed of 2.8 GHz. In comparison, Maheshwari et al. (2013) did simulations using a continuum-scale model (coupled to a pore-scale model) on a domain of 3.5cm x 1.4cm x 1.4cm (discretized to 150x60x60 cells) using a cluster of cores, and computing times ranged from 2-3h to

several days. As such, if this approach were to be developed to be able to accurately model these unstable dissolution patterns it would prove to be a very useful tool.

6 Conclusion

In conclusion, the developed model has shed light on several aspects pertaining to the dissolution of limestone at the pore-scale. While the model is not yet able to model the different dissolution regimes, it has shown the existence of optimum conditions for breakthrough, which is a trend reported throughout the literature. The novel formulation of the Damköhler number has been shown to accurately describe the optimum conditions for a variety of different simulation conditions, ranging from reaction-limited to mass-transfer limited. The next step would be to use the same definition and apply it to a variety of different types of models (direct and continuum models) and experiments.

Furthermore, from the results gathered in this research it was found that there was a dependency on the amount of calcite dissolved until breakthrough and the Damköhler number. This dependency shows a minimum and constant amount of calcite being dissolved for velocities ranging from the optimum conditions to fast flows. It would be interesting to see if this relationship persists for models and/or experiments that do show the various dissolution patterns. If so, it would also be interesting to investigate what factors influence the minimum porosity increase.

With respect to future work, a couple of key steps are outlined in order to be able to use this model as a predictive tool. First is to investigate the method of distribution of dissolved calcite and weighting of surface areas for each tube as it is believed that the secret to be able to model the varying dissolution patterns lies in these two aspects. The idea is to create an algorithm that accounts for the connectedness of throats. Second is to investigate the different factors that influence the PVBT and see whether the PVBTs obtained can be lowered while still being physically relevant. This could be through investigating the effect of factors mentioned previously: calcite density and the size of domain. It is already speculated that if propagation of dissolution fronts can be simulated realistically then this will reduce the PVBT. After that the next step would be to compare it to experiments and/or to fully integrated reactive pore-network model in which reactions are modelled within each throat. This would also entail the development of kinetic model that more convincingly accounts for mass-transfer limitations. While the model still has room for improvement, the approach does have its appeal. The key aspects that make this approach attractive are the ease of use and adaptability to different systems, and the vast reduction in computing cost. All these things make development of this approach worthwhile and a potentially valuable resource in reactive-transport modelling in porous media.

References

Acharya, R. C., et al. (2004). "Porosity–permeability properties generated with a new 2-parameter 3D hydraulic pore-network model for consolidated and unconsolidated porous media." Advances in Water Resources 27(7): 707-723.

Akervoll, I., et al. (2009). "Feasibility of Reproduction of Stored CO2 from the Utsira Formation at the Sleipner Gas Field." Energy Procedia 1(1): 2557-2564.

Akono, Ange-Therese et al. "A Review Of Geochemical–Mechanical Impacts In Geological Carbon Storage Reservoirs". *Greenhouse Gases: Science And Technology*, vol 9, no. 3, 2019, pp. 474-504. *Wiley*, doi:10.1002/ghg.1870.

Alkattan, M., et al. (1998). "An experimental study of calcite and limestone dissolution rates as a function of pH from y1 to 3 and temperature from 25 to 80C." Chemical Geology(151): 199–214.

Al-Kharusi, A. and M. J. Blunt (2006). "Permeability Prediction and Network Extraction from Pore Space Images."

Ameri, A., et al. (2017). "Detailed Modeling of Carbonate Acidizing by Coupling a Multi-Purpose Pore-Network Simulator to the Chemistry Package PHREEQC - Application to Chelating Agents." SPE.

Appelo, C. A. J., et al. (2014). "Equations for calculating hydrogeochemical reactions of minerals and gases such as CO2 at high pressures and temperatures." Geochimica et Cosmochimica Acta 125: 49-67.

Bijeljic, B., et al. (2013). "Insights into non-Fickian solute transport in carbonates." Water Resour Res 49(5): 2714-2728.

Blunt, M. J., et al. (2013). "Pore-scale imaging and modelling." Advances in Water Resources 51: 197-216.

Boot-Handford, M. E., et al. (2014). "Carbon capture and storage update." Energy Environ. Sci. 7(1): 130-189.

Charlton, S. R. and D. L. Parkhurst (2011). "Modules based on the geochemical model PHREEQC for use in scripting and programming languages." Computers & Geosciences 37(10): 1653-1663.

Chou, L., et al. (1989). "Comparative study of the kinetics and mechanisms of dissolution of carbonate minerals." Chemical Geology 78: 269-282.

Cohen, C. E., et al. (2008). "From pore scale to wellbore scale: Impact of geometry on wormhole growth in carbonate acidization." Chemical Engineering Science 63(12): 3088-3099.

Crank, J. (1975). The Mathematics of Diffusion. Oxford, Clarendon Press.

Daccord, G., et al. (1993). "Chemical Dissolution of a Porous Medium by a Reactive Fluid - I. Model for the "Wormholing" Phenomenon." Chemical Engineering Science 48(1): 169-178.

Fredd, C. N. and H. S. Fogler (1998). "Influence of Transport and Reaction on Wormhole Formation in Porous Media." AIChE Journal 44(9): 1933-1949.

Fredd, C. N. and H. S. Fogler (1998). "The kinetics of calcite dissolution in acetic acid solutions." Chemical Engineering Science 53(22): 3863-3874.

Freire-Gormaly, M., et al. (2015). "Pore Structure Characterization of Indiana Limestone and Pink Dolomite from Pore Network Reconstructions." Oil & Gas Science and Technology – Revue d'IFP Energies nouvelles 71(3).

Gao, J., et al. (2017). "Reactive transport in porous media for CO 2 sequestration: Pore scale modeling using the lattice Boltzmann method." Computers & Geosciences 98: 9-20.

Gharbi, O. and M. J. Blunt (2012). "The impact of wettability and connectivity on relative permeability in carbonates: A pore network modeling analysis." Water Resources Research 48(12).

Golfier, F., et al. (2001). "Acidizing Carbonate Reservoirs: Numerical Modelling of Wormhole Propagation and Comparison to Experiments." SPE.

Golfier, F., et al. (2002). "On the ability of a Darcy-scale model to capture wormhole formation during the dissolution of a porous medium." Journal of Fluid Mechanics 457: 213-254.

Gray, F., et al. (2018). "Chemical mechanisms of dissolution of calcite by HCl in porous media: Simulations and experiment." Advances in Water Resources 121: 369-387.

Hoefner, M. L. and H. S. Fogler (1988). "Pore Evolution and Channel Formation During Flow and Reaction in Porous Media." AIChE Journal 34(1): 45-54.

Jivkov, A. P., et al. (2013). "A novel architecture for pore network modelling with applications to permeability of porous media." Journal of Hydrology 486: 246-258.

Kalia, N. and V. Balakotaiah (2007). "Modeling and analysis of wormhole formation in reactive dissolution of carbonate rocks." Chemical Engineering Science 62(4): 919-928.

Kang, Q., et al. (2006). "Lattice Boltzmann pore-scale model for multicomponent reactive transport in porous media." Journal of Geophysical Research: Solid Earth 111(B5): n/a-n/a.

Koutsoukos, P. G. and C. G. Kontoyannis (1984). "Precipitation of Calcium Carbonate in Aqueous Solutions." J. Chem. Soc., Faraday Trans. 80(1): 1181-1192.

Levich, V. G. (1962). *Physicochemical Hydrodynamics*. Englewood Cliffs, N.J: Prentice-Hall. ISBN 0136744400

Li, L., et al. (2006). "Upscaling geochemical reaction rates using pore-scale network modeling."

Advances in Water Resources 29(9): 1351-1370.
Li, L., et al. (2007). "Applicability of averaged concentrations in determining geochemical reaction rates in heterogeneous porous media." American Journal of Science 307(10): 1146-1166.
Li, L., et al. (2008). "Scale dependence of mineral dissolution rates within single pores and fractures." Geochimica et Cosmochimica Acta 72(2): 360-377.
Maheshwari, P., et al. (2013). "3-D simulation and analysis of reactive dissolution and wormhole formation in carbonate rocks." Chemical Engineering Science 90: 258-274.
Mehmani, Y., et al. (2012). "Multiblock Pore-Scale Modeling and Upscaling of Reactive Transport: Application to Carbon Sequestration." Transport in Porous Media 95(2): 305-326.
Mostofizadeh, B., & Economides, M. J. (1994). "Optimum Injection Rate From Radial Acidizing Experiments". Society of Petroleum Engineers. doi:10.2118/28547-MS
Nogues, J. P., et al. (2013). "Permeability evolution due to dissolution and precipitation of carbonates using reactive transport modeling in pore networks." Water Resources Research 49(9): 6006-6021.
Ott, H. and S. Oedai (2015). "Wormhole formation and compact dissolution in single- and two-phase CO2-brine injections." Geophysical Research Letters 42(7): 2270-2276.
Panga, M. K. R., et al. (2005). "Two-scale continuum model for simulation of wormholes in carbonate acidization." AIChE Journal 51(12): 3231-3248.
Parkhurst, D. L. and C. A. J. Appelo (1999). User's guide to PHREEQC (Version 2) : a computer program for speciation, batch-reaction, one-dimensional transport, and inverse geochemical calculations. Water-Resources Investigations Report, U.S. Department of the Interior, U.S. Geological Survey.
Parkhurst, D. L. and C. A. J. Appelo (2013). Description of Input and Examples for PHREEQC Version 3—A Computer Program for Speciation, Batch-Reaction, One-Dimensional Transport, and Inverse Geochemical Calculations. Techniques and Methods, U.S. Department of the Interior U.S. Geological Survey: 497.
Parkhurst, D. L. and L. Wissmeier (2015). "PhreeqcRM: A reaction module for transport simulators based on the geochemical model PHREEQC." Advances in Water Resources 83: 176-189.
Peng, C., et al. (2015). "Kinetics of Calcite Dissolution in CO2-Saturated Water at Temperatures between (323 and 373) K and Pressures up to 13.8 MPa." Chemical Geology 403: 74-85.
Plummer, L. N., et al. (1978). "The Kinetics of Calcite Dissolution in CO2-Water Systems at 5-60C and 0.0-1.0 atm CO2." American Journal of Science 278: 179-216.
Plummer, L.Niel, and Eurybiades Busenberg. "The Solubilities Of Calcite, Aragonite And Vaterite In CO2-H2O Solutions Between 0 And 90°C, And An Evaluation Of The Aqueous Model For The System Caco3-CO2-H2O". *Geochimica Et Cosmochimica Acta*, vol 46, no. 6, 1982, pp. 1011-1040. *Elsevier BV*, doi:10.1016/0016-7037(82)90056-4.
Pokrovsky, O. S., et al. (2005). "Dissolution kinetics of calcite, dolomite and magnesite at 25 °C and 0 to 50 atm pCO2." Chemical Geology 217(3-4): 239-255.
Pokrovsky, O. S., et al. (2009). "Calcite, dolomite and magnesite dissolution kinetics in aqueous solutions at acid to circumneutral pH, 25 to 150 °C and 1 to 55 atm pCO2: New constraints on CO2 sequestration in sedimentary basins." Chemical Geology 265(1-2): 20-32.
Raoof, A. and S. M. Hassanizadeh (2009). "A New Method for Generating Pore-Network Models of Porous Media." Transport in Porous Media 81(3): 391-407.
Raoof, A. and S. M. Hassanizadeh (2010). "Upscaling Transport of Adsorbing Solutes in Porous Media." Journal of Porous Media 13(5): 395-408.
Raoof, A., et al. (2013). "PoreFlow: A complex pore-network model for simulation of reactive transport in variably saturated porous media." Computers & Geosciences 61: 160-174.
Raoof, A., et al. (2012). "Pore-scale modeling of reactive transport in wellbore cement under CO2 storage conditions." International Journal of Greenhouse Gas Control 11: S67-S77.
Selvadurai, A. P. S., et al. (2017). "Permeability of wormholes created by CO2-acidized water flow through stressed carbonate rocks." Physics of Fluids 29(9).
Sjoberg, E. L. (1976). "A fundamental equation for calcite dissolution kinetics." Geochimica et Cosmochimica Acta 40: 441-447.
Smith, M. M., et al. (2017). "Development and calibration of a reactive transport model for carbonate reservoir porosity and permeability changes based on CO 2 core-flood experiments." International Journal of Greenhouse Gas Control 57: 73-88.
The Core Writing Team (2014). Climate Change 2014 Synthesis Report. IPCC 2014. R. K. Pachauri and L. Meyer. Geneva, IPCC.
Wang, Y., Hill, A. D., & Schechter, R. S. (1993). "The Optimum Injection Rate for Matrix Acidizing of Carbonate Formations". Society of Petroleum Engineers. doi:10.2118/26578-MS
Wolterbeek, T. K. T. and A. Raoof (2018). "Meter-Scale Reactive Transport Modeling of CO2-Rich Fluid Flow along Debonded Wellbore Casing-Cement Interfaces." Environ Sci Technol 52(6): 3786-3795.
Xiong, Q., et al. (2016). "Review of pore network modelling of porous media: Experimental characterisations, network constructions and applications to reactive transport." J Contam Hydrol 192: 101-117.

Zheng, L., et al. (2019). "When can the local advection–dispersion equation simulate non-Fickian transport through rough fractures?" Stochastic Environmental Research and Risk Assessment 33(3): 931-938.

Appendix

A1: Main Executable File (.bat)

```
@echo off
setlocal enabledelayedexpansion
REM                                    ###  GENERAL DESCRIPTION ###
REM This batch file includes the code to run the coupled reactive transport model. The model uses two existing models,
REM PoreFlow and PHREEQC, to achieve this. Each model is in its own directory, in which they have their respective
REM input and output files. The input PoreFlow requires from PHREEQC is the amount of kinetically dissolved
REM calcite, which is found in the text file delCalcite.txt. The input PHREEQC requires from PoreFlow is the
REM total area of each segment of the pore structure, which is found in PHREEQC_CELL_INFO.TXT. Lines 12-1 are
REM the code used for the initialization of the model, creating/generating the necessary initial input files.
REM The lines thereafter actually run the model for the desired number of timesteps given in line 14.

REM Prompt for timesteps
echo.
set /p x=Enter number of timesteps:
REM Prompt for initial number of moles of calcite (per segment/cell)
echo.
REM set /p initial_moles=Enter initial number of moles of calcite per segment:
set initial_moles=176.85
echo.
REM Start timer
call :START

REM Delete results from previous run
del /f/q poreflow\RESULTS\*
del /f/q phreeqc\CSV\*
del /f/q poreflow\RESULTS\SELECTED_OUTPUT\*

::-----------------------------------------------------------------------------------------------------------------------
::Generate Pore-Network (comment this section if the network generation is not needed)
::-----------------------------------------------------------------------------------------------------------------------
REM Initially the pore-network needs to be generated for a given initial pore-size (PORER) distribution. This is
REM done in the following section. Two seperate PoreFlow input files (poreflow.in) exist, one for network generation
REM and one used in the loop. Each is in a seperate directory, along with other necessary input files, allowing
REM to easily to move all the contents of a desired folder into the working INPUTS directory which poreflow uses.

REM REM First, delete the current contents in the working INPUTS folder
REM del /f/q poreflow\INPUTS\*
REM REM Rename the original pore (body) radius distribution to PORER
REM copy /y poreflow\INPUTS\inputs_for_gen\pore_size_ORIGINAL.txt poreflow\INPUTS\inputs_for_gen\PORER.txt
REM REM Copy all contents from "inputs_for_gen" folder into INPUTS
REM copy /y poreflow\INPUTS\inputs_for_gen\* poreflow\INPUTS
REM REM Now run poreflow to generate the full initial pore-network
REM cd poreflow\PoreFlow\PoreFlow
REM call poreflow_win10
REM REM Copy necessary files from the RESULTS folder into the "inputs_for_loop" folder
REM cd ..\..
REM copy /y RESULTS\PORER_0.txt INPUTS\inputs_for_loop\PORER.txt
REM copy /y RESULTS\PIPEL_0.txt INPUTS\inputs_for_loop\PIPEL.txt
REM copy /y RESULTS\PIPER_0.txt INPUTS\inputs_for_loop\PIPER_INITIAL.txt
REM copy /y RESULTS\PIPER_0.txt INPUTS\inputs_for_loop\PIPER.txt
REM copy /y RESULTS\Qij_0.txt INPUTS\inputs_for_loop\Qij_INITIAL.txt
REM copy /y RESULTS\Qij_0.txt INPUTS\inputs_for_loop\Qij.txt
REM copy /y RESULTS\CONF.txt INPUTS\inputs_for_loop
REM copy /y RESULTS\PORE_LOC.txt INPUTS\inputs_for_loop
REM copy /y RESULTS\PORE_INLET.txt INPUTS\inputs_for_loop
REM REM Delete contents of RESULTS folder
REM del /f/q RESULTS\*
REM REM Change back to original directory
REM cd ..

::-----------------------------------------------------------------------------------------------------------------------
::Initialize PHREEQC
::-----------------------------------------------------------------------------------------------------------------------
REM Remove current files in the INPUTS folder and then copy all files from "inputs_for_loop" into INPUTS
del /f/q poreflow\INPUTS\*
copy /y poreflow\INPUTS\inputs_for_loop\* poreflow\INPUTS
REM Do the same for the phreeqc inputs; delete current contents from \phreeqc and copy the contents from
REM \phreeqc\inputs into \phreeqc
del /f/q phreeqc\*
copy /y phreeqc\inputs\* phreeqc

REM PHREEQC requires as input the mean radius and total surface area of each segment defined in PoreFlow
REM (in PHREEQC_CELL_INFO.TXT), and so initially PoreFlow needs to be run to get this information. However,
REM PoreFlow requires delCalcite.txt as input, and thus an initial delCalcite.txt is made in which all the
REM values for kinetically dissolved calcite are set to zero, and is copied to poreflow\INPUTS
copy /y phreeqc\delCalcite_initial.txt poreflow\INPUTS\delCalcite.txt

REM Set run_counter to zero
cd poreflow\INPUTS
echo 0 > poreflow_run_counter.txt

REM Run PoreFlow to generate PHREEQC_CELL_INFO.TXT for zero delCalcite!
cd ..\PoreFlow\PoreFlow
call poreflow_win10

REM Copy PHREEQC_CELL_INFO.TXT is outputted and copy it to the phreeqc directory.
cd ..\..\RESULTS
copy /y PHREEQC_CELL_INFO.TXT ..\..\phreeqc

REM Copy initial conditions to dump files which will be used in PHREEQC with the INCLUDE$ keyword.
REM The dump files will be overwritten with every run!
cd ..\..\phreeqc
copy /y initial_dump1.dmp dump.dmp
copy /y initial_trans1.dmp trans.dmp
copy /y initial_porosities.txt porosities.txt

REM Creating KINETIC datablock for each cell (no values for parameters yet!)
REM This is done in Batch because when done in PHREEQC as: KINETICS 1-20... the k_modify (created below) does not
REM modify the KINETICS data block for all the cells properly, which is necessary to include the initial average
REM radius and total surface area of each segment of the pore structure. As such the KINETICS data block, created
REM in Batch, is appended to the dump.dmp file which already includes the initial SOLUTION data block. This is all
REM done in the subroutine ":kinetics_datablock", with the first argument being the initial number of moles of calcite.
call :kinetics_datablock %initial_moles%

REM Create k_modify.txt (which will include the parameters for the above KINETICS data blocks). k_modify.txt will be
REM included in the phreeqc input file using INCLUDE$, essentially modifying the above KINETICS data block with the
```

```
REM necessary parameters (radius, area, and surface activites from the previous timestep) from PoreFlow (i.e.
REM PHREEQC_CELL_INFO.TXT). This is all done in the subroutine ":kinetics_modify".
call :kinetics_modify1

::--------------------------------------------------------------------------------------------------------------------
IF !x! GTR 0 (
		echo.
		echo ====================================================
		echo ============STARTING REACTIVE TRANSPORT==============
		echo ====================================================

		REM Now that the initialization has been done, we run PHREEQC and PoreFlow for every timestep; first PHREEQC then PoreFlow.
		REM looping over number of timesteps
		for /l %%i in (1, 1, %x%) do (
			echo.
			echo ----------TIMESTEP %%i----------
			echo.

			call :header_PCI "Starting porosities for PHREEQC run"
			call :selected_output 1 "porosities.txt" "PHREEQC_CELL_INFO"

			REM run PHREEQC; input file is Phrqc_diff.pqi
			call phreeqc Phrqc_diff.pqi
			REM Update the porosities.txt file from outputted file porosities_temp.txt
			call :update_porosities
			REM Create new k_modify.txt file that updates the m0 for each loop
			call :kinetics_modify2
			REM Create CSV files to be viewed in ParaView; porosity, pH, and Calcite. This is done using subroutine ":create_csv"
			call :create_csv %%i "porosities_temp.txt" "porosity_0" "porosity_1" "porosity_%%i"
			call :create_csv %%i "pH_temp.txt" "pH_0" "pH_1" "pH_%%i"
			call :create_csv %%i "delCalcite.txt" "Calcite_0" "Calcite_1" "Calcite_%%i" %initial_moles%
			call :create_csv %%i "concentrations_temp.txt" "Concentrations_0" "Concentrations_1" "Concentrations_%%i"
			REM Copy output from phreeqc to poreflow input file
			copy /y delCalcite.txt ..\poreflow\INPUTS
			REM run PoreFlow
			cd ..\poreflow\PoreFlow\PoreFlow
			call poreflow_win10
			REM change to directory with PHREEQC_CELL_INFO.TXT
			cd ..\..\RESULTS
			REM copy PHREEQC_CELL_INFO.TXT to phreeqc input directory
			copy /y PHREEQC_CELL_INFO.TXT ..\..\phreeqc
			REM change back to phreeqc directory
			cd ..\..\phreeqc
		)

		REM Output network porosity and conductivity calculated by poreflow for each timestep
		REM Go to directory with porosity and conductivity info
		cd ..\poreflow\RESULTS
		REM Copy porosity data from INFO_0.txt
		call :selected_output 6 "INFO_0.txt" "SELECTED_OUTPUT\porosity"
		call :selected_output 4 "INFO_0.txt" "SELECTED_OUTPUT\conductivity"
		call :selected_output 2 "INFO_0.txt" "SELECTED_OUTPUT\Q_in"
		call :selected_output 9 "INFO_0.txt" "SELECTED_OUTPUT\min_piper"
		call :selected_output 10 "INFO_0.txt" "SELECTED_OUTPUT\max_piper"
)
REM Stop timer and show total run time
echo.
echo.
call :END
echo NUMBER OF TIMESTEPS: %x%
call :ShowDiff n

exit /b

::--------------------------------------------------------------------------------
REM The next section is for subroutines used in the code
::--------------------------------------------------------------------------------
REM Subroutine to create kinetics datablock
:kinetics_datablock
for /l %%i in (1, 1, 20) do (
		echo. >> dump.dmp
		echo KINETICS %%i >> dump.dmp
		echo Calcite >> dump.dmp
		echo -tol   1e-8 >> dump.dmp
		echo -bad_step_max 100000 >> dump.dmp
		REM Following line includes the initial amount of calcite
		echo -m0    %1 >> dump.dmp
		echo -parms >> dump.dmp
)
exit /b
REM Subroutine to create kinetics_modify.txt
:kinetics_modify1
echo. > k_modify.txt
REM loop over number of cells\segments
for /l %%i in (1, 1, 20) do (
		echo KINETICS_MODIFY %%i >> k_modify.txt
		REM line to include output file from PoreFlow
		echo INCLUDE$ PHREEQC_CELL_INFO.TXT >> k_modify.txt
		echo. >> k_modify.txt
)
exit /b
REM Subroutine to create new kinetics_modify.txt file to account for changing m0
:kinetics_modify2
echo. > k_modify.txt
for /l %%k in (1, 1, 20) do (
		echo KINETICS_MODIFY %%k >> k_modify.txt
		echo INCLUDE$ PHREEQC_CELL_INFO.TXT >> k_modify.txt
		set /a line=0
		FOR /F "tokens=1 usebackq" %%G IN ("delCalcite.txt") DO (
			set /a line+=1
			set /a bingo=21+%%k
			IF !line! EQU !bingo! (
			echo -m0    %%G >> "k_modify.txt")
		)
		echo. >> k_modify.txt
)
exit /b
REM Subroutine to create new header in PHREEQC_CELL_INFO.TXT
:header_PCI
echo ################################### >> "PHREEQC_CELL_INFO.TXT"
echo #%~1 >> "PHREEQC_CELL_INFO.TXT"
echo ################################### >> "PHREEQC_CELL_INFO.TXT"
exit /b
REM Subroutine to update porosities in porosities.txt from porosities_temp
```

```
:update_porosities
echo -porosities > porosities.txt
set /a line=0
FOR /F "tokens=1 usebackq" %%G IN ("porosities_temp.txt") DO (
		set /a line+=1
		IF !line! GTR 21 (
		echo %%G >> "porosities.txt")
)
exit /b
REM Subroutine to create CSV files
:create_csv
if %1==1 (
		set /a line=0
		for /F "tokens=* usebackq" %%G in ("%~2") do (
			set /a line+=1
			if !line! LEQ 21 if !line! GTR 1 (
				echo %%G >> "CSV\%~3.csv")
			if !line! GTR 21 (
				echo %%G >> "CSV\%~4.csv")
		)
		if "%~2" == "delCalcite.txt" (
			for /l %%i in (1, 1, 20) do (
				if %%i EQU 1 (
					echo %6	0 > "CSV\%~3.csv")
				if %%i GTR 1 (
					echo %6	0 >> "CSV\%~3.csv")
			)
		)
) else (
		set /a line=0
		for /F "tokens=* usebackq" %%G in ("%~2") do (
			set /a line+=1
			if !line! GTR 21 (
				echo %%G >> "CSV\%~5.csv")
		)
)
exit /b
REM Subroutine to create files for selected_output (e.g. porosity and conductivity)
:selected_output
for /F "tokens=%1 skip=1 usebackq" %%G in ("%~2") do (
		echo %%G >> "%~3.txt"
)
exit /b
REM The following code is from Stephen Knight (2012), Dragon Computer Consulting
REM ========================================
REM Subroutines to calculate run time are below
REM ========================================
:START
set start=%date% %time:~0,8%
REM echo START at %start%
exit /b

:END
set end=%date% %time:~0,8%
REM echo END at %end%
exit /b

:ShowDiff
REM Call with s,n,h for seconds, mins, hours. defaults to secs
(set type=%~1)& if "%~1"=="" set type=s

echo Wscript.Echo DateDiff("%type%", #%start%#,#%end%# ) > "%temp%\timediff.vbs"
for /f %%s in ('cscript //nologo "%temp%\timediff.vbs"') do set TimeDiff=%%s
del "%temp%\timediff.vbs"
if %Type%==n set type=m
echo TOTAL TIME TAKEN: %TimeDiff% %Type%
exit /b

endlocal
```

A2: Main PHREEQC Input File

```
########################################################################
# 1D kinetic dissolution model of calcite due to low pH solution injection
# Naod Negash and Flor Wassing
# 15-04-2019
########################################################################

#Create injection solution with pure water in equilibrium with CO2
SOLUTION 0 Injection fluid in eq. with CO2 #such that pH~3.5
    temp      50
    pH        7 charge
    pe        4
    redox     pe
    units     mol/kgw
    density   1
    -water    1 # kg
EQUILIBRIUM_PHASES 0
    CO2(g)    2 10 # pCO2 = 10^2 atm
SAVE SOLUTION 0
END


#Reading SOLUTION 1-20 and KINETICS 1-20 from dump.dmp
#Initially the dump.dmp include SOLUTION and KINETICS datablocks but will be rewritten to a _RAW format after the first run.
INCLUDE$ dump.dmp

#Include k_modify.txt which modifies each KINETICS datablock to include the parameters in PHREEQC_CELL_INFO.TXT. The file
#PHREEQC_CELL_INFO.TXT consists of a list of parameters for each cell (i.e. first 20 are the average pipe radius, next 20 are
#average pipe length etc.)
INCLUDE$ k_modify.txt

#The following RATES datablock includes our rate equation for calcite dissolution. Basic lines 1 and 2 read the average radius and
#total reactive surface area for each cell from the parameters defined in PHREEQC_CELL_INFO.TXT. If statement at line 100 states the
#rate=0 if the saturation index is =0. The rate below is for the reaction-limited rate expression.
RATES
Calcite
 -start
1  R = PARM(CELL_NO)                                          #average radius for cell [m]
2  A = PARM(CELL_NO+40)                                       #total reactive surface area [m^2]

10 k1T25 = 0.89                                               #rate constant mol/m2/s (Chou et al., 1989)
11 k2T25 = 5.01*10^(-4)                                       #(Chou et al., 1989)
12 k3T25 = 6.6*10^(-7)                                        #(Chou et al., 1989)

20 Ea1 = 8.37                                                 #activation energy kJ/mol (Plummer et al., 1978)
21 Ea2 = 41.88                                                #(Plummer et al., 1978)
22 Ea3 = 33.08                                                #(Plummer et al., 1978)
23 Rc = 8.314e-3                                              #ideal gas constant kJ/mol/K

30 k1 = k1T25*EXP((Ea1/Rc)*((1/298.15)-(1/TK))) #new rate constants accounting for temperature
31 k2 = k2T25*EXP((Ea2/Rc)*((1/298.15)-(1/TK)))
32 k3 = k3T25*EXP((Ea3/Rc)*((1/298.15)-(1/TK)))

40 Ksp = 10^LK_PHASE("Calcite")                               #equilibrium constant calcite [-] (PHREEQC database; Plummer and
Busenberg, 1982)

50 aH = ACT("H+")
51 aH2CO3 = ACT("CO2")
52 aCO3 = ACT("CO3-2")
53 aCa = ACT("Ca+2")

100 si_cc=LOG10(aCa*aCO3/Ksp)
101 IF (si_cc = 0) THEN GOTO 250

120 rate = (k1*aH + k2*aH2CO3 + k3)*(1-((aCa*aCO3)/Ksp)) #Specific rate (mol/m2/s)
130 moles = rate * TIME * A

#calculate new porosity
140 ini_por = PARM(CELL_NO+80)
141 tot_moles = M0/(1 - ini_por)
142 dmol = (M0-M)
143 dPor = dmol/tot_moles
144 new_por = ini_por + dPor
145 CHANGE_POR(new_por,CELL_NO)

250 SAVE moles
 -end

#Reading TRANSPORT datablock from trans.dmp and reading cell porosities from porosities.txt
INCLUDE$ trans.dmp
INCLUDE$ porosities.txt

#Dumping new solution composition and kinetic data in _RAW format (-.dmp is overwritten)
DUMP
-file dump.dmp
-append false
-solution 1-20
-kinetics 1-20

#Output concentrations (molalities) of given species
SELECTED_OUTPUT 1
                -file                           concentrations_temp.txt
                -reset                          false
                -high_precision         true
                -solution               true
                -time                           true
                -step                           true
                -molalities             H+      OH-     Ca+2 CO3-2  CO2     HCO3-

#Output the pH in each cell, used for the generation of CSV files to view pH development in the network over time.
SELECTED_OUTPUT 2
    -file                               pH_temp.txt
                -high_precision         true
                -reset                  false
                -solution               false
                -pH                                     true

#USER PUNCH allows us to choose what values we want to send to the selected output from the Basic environment, in this case the
#porosities.
USER_PUNCH 3
```

```
                -headings -porosities
 -start
10 PUNCH GET_POR(CELL_NO)
 -end

SELECTED_OUTPUT 3
                -file                                   porosities_temp.txt
                -high_precision true
                -reset                                  false
                -user_punch             true

#Output the amount of kinetically dissolved/precipitated calcite to delCalcite.txt, which is used as input for PoreFlow. This file
#will also serve as a source for the creation of CSV files to track the development of amount of calcite in each cell, allowing it
#to be viewed in ParaView.
USER_PUNCH 4
                -headings k_Calcite dk_Calcite
 -start
10 PUNCH M
20 PUNCH M-M0
 -end

SELECTED_OUTPUT 4
                -file                                   delCalcite.txt
                -high_precision true
                -reset                                  false
                -user_punch             true

PRINT
                -reset          false

END
```

A3: PHREEQC Input file – *initial_dump.dmp*

The following code contains the initial background solution, and gets updated during a run such that each time PHREEQC is called it retains the speciation from before PoreFlow is called.

```
SOLUTION 200 Background solution in eq. with calcite #initially filling column
    temp      50
    pH        7 charge
    pe        4
    redox     pe
    units     mol/kgw
    density   1
    -water    1 # kg
EQUILIBRIUM_PHASES 200
                Calcite 0 # SI(Calcite) = 0
SAVE SOLUTION 1-20
END # not including this END statement affects results!
```

A4: PHREEQC Input file – *initial_trans.dmp*

The following code contains the TRANSPORT datablock used in PHREEQC. It is defined externally since it is easier to manipulate.

```
TRANSPORT
    -cells                  20
    -shifts                 2000
    -time_step              0.002 # seconds
    -lengths                0.0016 # meter
    -dispersivities         0.00016
    -correct_disp           true
    -punch_cells            1-20
    -punch_frequency        2000
    -multi_d                true 1e-09 0.13 0 1
```

A5: Pore-body and -throat radii distribution

The following distributions are for the pore body and throat radii for the generated network.

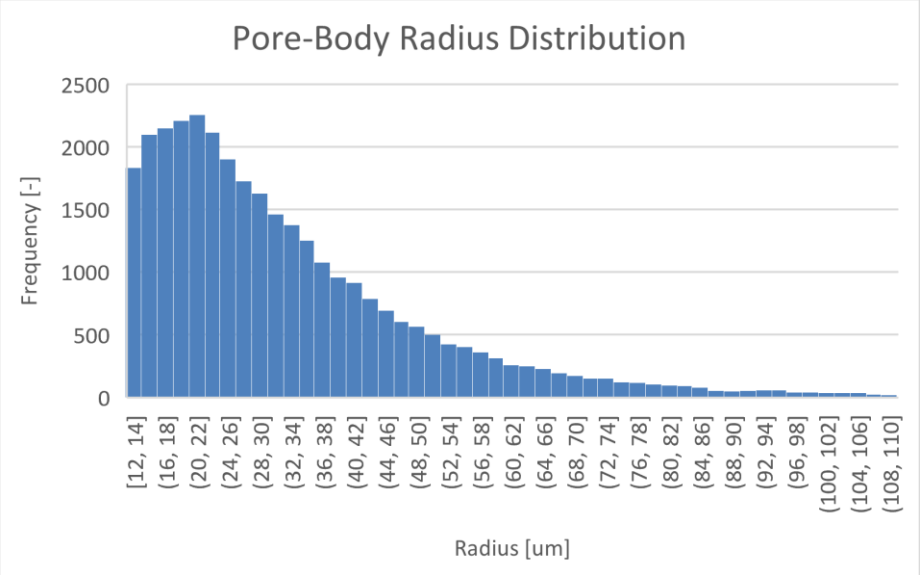

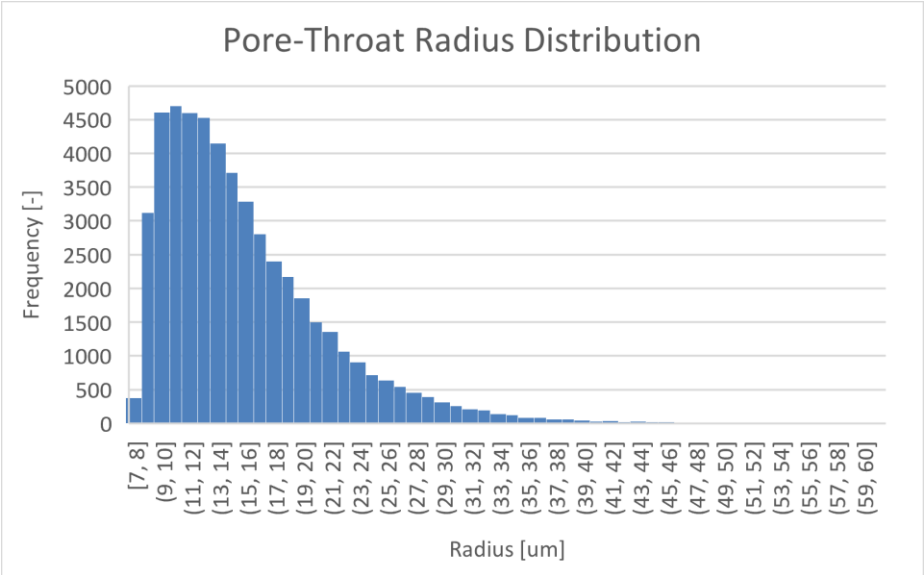

A6: Derivation of mass-transfer limited rate expression

The diffusive flux is based on the steady-state hollow cylinder diffusion model by Crank (1975). To start, the diffusion equation for steady-state radial diffusion in a long hollow cylinder with inner radius r_1 and outer radius r_2 is given by:

$$\frac{d}{dr}\left(r\frac{dC}{dr}\right) = 0, \qquad r_1 < r < r_2 \tag{A6.1}$$

With boundary conditions $C(r_1) = C_1$ and $C(r_2) = C_2$ the following equation for concentration as a function of radius is obtained:

$$C(r) = \frac{C_1 \ln\left(\frac{r_2}{r}\right) + C_2 \ln\left(\frac{r}{r_1}\right)}{\ln\left(\frac{r_2}{r_1}\right)} \tag{A6.2}$$

Differentiating this then gives:

$$\frac{dC}{dr} = \frac{C_2 - C_1}{\ln\left(\frac{r_2}{r_1}\right)}\frac{1}{r} \tag{A6.3}$$

Leading to the diffusive flux (Fick's first law) being defined as:

$$J(r) = -D\frac{dC}{dr} = -D\frac{C_2 - C_1}{\ln\left(\frac{r_2}{r_1}\right)}\frac{1}{r} \tag{A6.4}$$

In equation A6.4 C_1 and C_2 correspond to the bulk and surface concentration, respectively, with the surface concentration being assumed as the equilibrium concentration since it is assumed to be mass-transfer limited. Furthermore, following Raoof and Hassanizadeh (2010) the bulk concentration is assumed at $r_1 = R/2$, where R is radius of the tube, and the outer boundary is $r_2 = R$. Thus, the flux at the boundary r = R is given by:

$$J(R) = -D\frac{C_{eq} - C_{bulk}}{\ln(2)}\frac{1}{R} \tag{A6.5}$$

This expression is then used as the rate expression for the mass-transfer limited reaction.